Impact of Correlated RF Noise on SiGe HBT
Noise Parameters and LNA Design Implications

by

Xiaojia Jia

A thesis submitted to the Graduate Faculty of
Auburn University
in partial fulfillment of the
requirements for the Degree of
Master of Science

Auburn, Alabama
December 14, 2013

Keywords: SiGe HBT, RF noise, LNA design, technology scaling

Approved by

Guofu Niu, Alumni Professor of Electrical and Computer Engineering
Fa Foster Dai, Professor of Electrical and Computer Engineering
Stuart Wentworth, Associate Professor of Electrical and Computer Engineering

Abstract

This work presents analytical models of SiGe HBT and LNA noise parameters accounting for high frequency noise correlation. The models are verified using measurement data and circuit simulation. The impact of noise correlation is shown to be a strong function of base resistance r_b which acts as both a noise source and an impedance. Correlation and r_b as impedance have opposite effects on minimum noise figure NF_{min}, which explains why a widely used NF_{min} model that neglects correlation and r_b as impedance agreed with measurements. The agreement, however, does not hold for noise matching source resistance R_{opt}, an important parameter for LNAs. With correlation, noise matching condition is better met for impedance matched LNAs.

Acknowledgments

Foremost, I would like to express my sincere gratitude to my advisor Dr. Guofu Niu, for his patience, assistance and guidance throughout the process of writing this thesis. Without his help this work would not haven been possible. I appreciate his immense knowledge and skills that helped me in all the time of research and this thesis.

Besides my advisor, I would like to thank the rest of my thesis committee members, Dr. Fa Dai, and Dr. Stuart Wentworth, for their encouragement, insightful comments, and helpful suggestions.

I would like to extend my sincere gratitude to former and current labmates in our SiGe HBT research group. I would like to thank Zhen Li for his patient instructions and constant help that are important to my academic growth. Many thanks also go to Ruocan Wang, Jingshan Wang, Wei-Chung Shih, Jingyi Wang, Zhenyu Wang, Pengyu Li, and Rongchen Ma, for the days and nights we were working together, and for all the fun we have had in the last two years. Also, I would like to thank my friends and everyone else who helped me in completion of this work.

Last but not the least, I would like to thank my parents, for their selfless support, understanding and love that protect me and give me courage to face any difficulties throughout my life.

Table of Contents

Abstract ii

Acknowledgments iii

List of Figures vi

List of Tables viii

1 Introduction 1

1.1 Motivation 1

1.2 SiGe HBT fundamental 2

1.3 Thesis Structure 4

2 Noise in Semiconductor 5

2.1 Thermal Noise 6

2.2 Terminal Current Noise 6

2.2.1 SPICE Noise Model 6

2.2.2 Correlation Noise Model 6

3 Analytical Derivation of Noise Parameters 9

3.1 Noise Parameters of LNA 9

3.2 Device Noise Parameters and Relations to LNA Noise Parameters 16

4 Impact of Correlation on Device Noise Parameters 17

4.1 Analytical Model Verification 17

4.2 Correlation's Impact on R_{opt}^{Device} 19

4.3 Correlation's Impact on F_{min}^{Device} 19

4.4 Correlation's Impact on X_{opt}^{Device} 20

4.5 Correlation's Impact on R_{n}^{Device} 21

4.6 Two Roles of r_b 22

4.7 Correlation and r_b Interaction 25
5 LNA Design Implication 27
6 Technology Scaling 31
7 Conclusion 34
Bibliography 35
Appendices 38
A Derivation of Intrinsic Noise Sources' Contributions to i_{out}: i_{out}^{c}, i_{out}^{b}, i_{out}^{rb}, and i_{out}^{Rs} . . . 39
A.0.1 i_{out}^{c}: 39
A.0.2 i_{out}^{b}: 40
A.0.3 i_{out}^{rb}: 41
A.0.4 i_{out}^{Rs}: 41
B Matlab Code for Noise Parameters of Device Calculation 43
C Matlab Code for Noise Parameters of Matched LNA 48

List of Figures

1.1 Simplified schematic of the LNA consisting of a single SiGe HBT. 2

1.2 Energy band diagrams of a graded-base SiGe HBT and an Si BJT [25][27]. 3

2.1 RF noise sources of a transistor. 5

2.2 1-D bipolar transistor with collector-base space charge region (CB SCR) effect [8]. . 7

2.3 PSD of i_b and i_c using correlation model and SPICE model versus Frequency, J_C=0.414 mA/μm^2, τ_n=0.651E-12 sec, f_T=50GHz. 8

3.1 Simplified small signal equivalent circuit of LNA. 10

3.2 Equivalent circuit of simplified LNA without power source. 14

3.3 Equivalent small signal circuit of simplified LNA without noise sources. 15

4.1 Analytical, simulated and measured noise parameters of SiGe HBT with A_E=0.8×20×3 μm^2 versus J_C at V_{CE}=3.3 V, f=5 GHz. 18

4.2 Device noise resistance R_n normalized by 50 Ω. 21

4.3 Analytical and measured noise parameters of SiGe HBT device versus frequency at V_{CE}=3.3 V, I_c=3.47 mA. 22

4.4 r_b's impact on NF_{min} of device versus frequency at V_{CE}=3.3 V, I_c=3.47 mA. 23

4.5 r_b's impact on R_{opt} of device versus frequency at V_{CE}=3.3 V, I_c=3.47 mA. 24

4.6 r_b's impact on X_{opt} of device versus frequency at V_{CE}=3.3 V, I_c=3.47 mA. 24

4.7 (a) NF_{min}^{Device} versus J_C at 5 GHz; (b) R_{opt}^{Device} versus J_C at 5 GHz. 25

4.8 $F_{min} - 1$ versus frequency at J_C=6.62 mA/μm^2. 26

5.1 R_{opt}^{LNA}, X_{opt}^{LNA}, NF_{min}^{LNA}, and NF^{LNA} of impedance matched LNA versus L_E at J_C=0.158 mA/μm^2, f=5 GHz 28

5.2 NF_{min}, NF, R_{opt}, X_{opt}, and corresponding L_E and I_C of LNAs using SPICE model and correlation model versus J_C at 5GHz. 29

6.1 f_T, NF_{min}^{Device}, and $r_b \times g_m$ versus J_C of three technology devices. 32

6.2 NF_{min}^{Device} and $R_{opt}^{Device} \cdot L_E$ versus $r_b \times g_m$ of three technology devices. 33

6.3 In LNA design, L_E, I_C, and J_C versus lithography node. 33

A.1 Simplified small signal equivalent circuit of LNA 39

A.2 Simplified small signal equivalent circuit of LNA with intrinsic current noise source i_c. 40

A.3 Simplified small signal equivalent circuit of LNA with intrinsic current noise source i_b. 40

A.4 Simplified small signal equivalent circuit of LNA with thermal noise source v_{rb}. 41

A.5 Simplified small signal equivalent circuit of LNA with thermal noise source v_{Rs}. 42

List of Tables

4.1 S_{ibib^*}, S_{icic^*}, S_{icib^*}, and S_{ibic^*} of Correlation model and SPICE model 17

6.1 Main Features of Three Technologies 31

Chapter 1

Introduction

1.1 Motivation

High frequency noise correlation has been shown to be important for accurate modelling of transistor noise parameters, in particular, minimum noise figure NF_{min} is smaller with correlation [1][2][3][4][5][6][7][8][9]. Recently the impact of noise correlation on LNA design was investigated using ADS simulation [10]. However, accurate analytical equations that express transistor and LNA noise parameters in terms of small signal equivalent circuit parameters like cut-off frequency f_T, transconductance g_m, and base resistance r_b have yet to be developed using correlated noise model.

The most used analytical transistor noise parameter expressions [11][12][13] are derived with varying degree of approximations using the so-called SPICE noise model, which models base and collector current noises as uncorrelated shot noises. These equations have been widely used in both device technology development [14][15][16] and circuit design [12][17]. Transistor noise parameter expressions were derived in [1] and [7] by introducing correlation. However, the base current noise was still assumed to be shot like, while more recent experimental extractions [6][18][19] and impedance field based analysis of modern SiGe HBTs [20] show a strong and clear frequency dependence in base current noise. The $2qI_B$ shot noise component is a result of emitter minority hole velocity fluctuations, and is not correlated to the collector current noise [21][22]. It is the frequency dependent component of base current noise that correlates with collector current noise.

This work aims to develop new expressions using a recent transistor correlation noise model [8][23] that accounts for frequency dependent base current noise. As the primary application is low-noise amplifier (LNA) design, derivation is made directly on a LNA as shown in Fig. 1.1. Transistor results are then obtained as a special case by setting the matching inductances to zero. This allows an easier inspection of the relationship between transistor and LNA noise parameters, as well as how it is affected by noise correlation.

In particular, the new expressions will be used to investigate how correlation affects transistor noise parameters and the nice transistor property of being able to approximately achieve simultaneous LNA noise and impedance matching, which was obtained using the SPICE noise model [12][24]. The Z_s in Fig. 1.1 is in general equal to R_s, 50Ω, with a reactance X_s=0. Transistor size can be optimized for noise matching source resistance R_{opt}=50Ω, or real part noise matching. Emitter and base inductors L_e and L_b can then be adjusted for R_{in}=50Ω, X_{in}=0, or real part and imaginary part impedance matching. The resulting noise matching source reactance $X_{opt} \approx X_s = 0$, or imaginary part noise matching. A logical question is if such property still holds with correlation, and if so, how transistor size and LNA noise figure are affected.

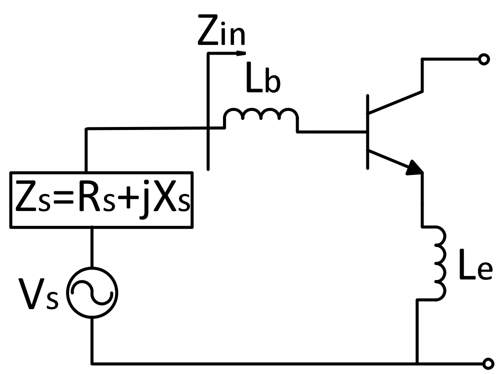

Figure 1.1: Simplified schematic of the LNA consisting of a single SiGe HBT.

1.2 SiGe HBT fundamental

SiGe heterojuction bipolar transistor (HBT) technology is extensively used to develop electronics for low noise operation due to its excellent analog and RF performance. The SiGe HBT technology is the first practical bandgap engineering device realized in silicon and can be integrated with the modern CMOS technology. As a result of introducing the graded Ge layer into the base of bipolar junction transistor (BJT), SiGe HBT technology has better performance than traditional Si BJT in DC, RF, and noise performance [25][13]. To illustrate the difference between the SiGe HBT and the Si BJT, Fig. 1.2 shows the energy-band diagrams for both the the SiGe HBT and the Si BJT biased identically in forward-active mode. The Ge profile linearly increases from zero near emitter-base (EB) junction to some maximum value near collector-base (CB) junction, and then rapidly ramps down to zero. This graded-Ge results in an extra drift field in the neutral base. The induced drift field accelerates minority carrier transportation, thus it minimizes transit time and increases cut-off frequency [26]. Because of this advantage and low noise performance, SiGe HBTs have been widely used in commercial and military wireless communication applications.

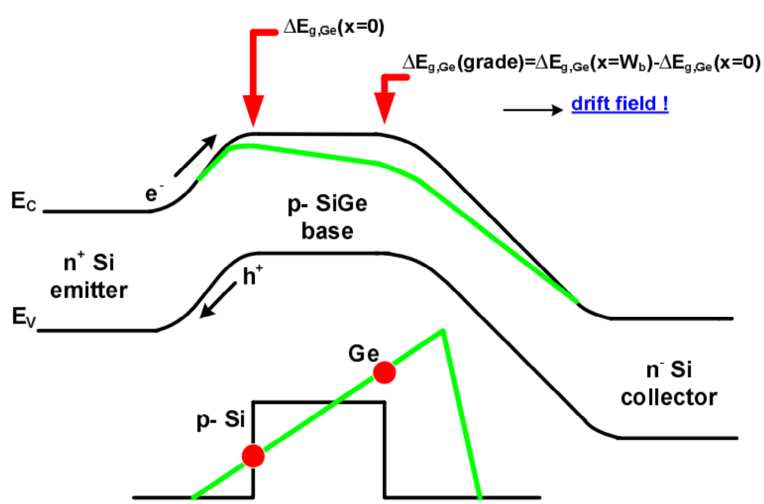

Figure 1.2: Energy band diagrams of a graded-base SiGe HBT and an Si BJT [25][27].

1.3 Thesis Structure

The work is organized as follows. Chapter 1 gives the motivation of this work as well as an overview of SiGe HBT technology. Chapter 2 presents thermal noise and intrinsic current noises in semiconductor. Derivations of noise parameters are made in Chapter 3. Small signal equivalent circuit analysis is used instead of linear noise two port analysis to better track how each noise source or equivalent circuit parameter, e.g. r_b, enters the final noise parameter expressions. While r_b as a thermal noise source is well appreciated, its role as an impedance is often neglected, e.g. in [12][13][28]. In Chapter 4, we verify the model equations with measurement and simulation, and examine how correlation affects transistor noise parameters, as well as the two roles of r_b. The role of r_b as impedance is shown to be important. Chapter 5 discusses LNA design implications, followed by technology scaling discussions in Chapter 6. Chapter 7 concludes the work.

Chapter 2

Noise in Semiconductor

The operation of semiconductor devices is based on free carriers transportation [29]. From the equivalent circuit and compact modeling stand point, the velocity fluctuation caused by majority carrier thermal motion can be expressed by the thermal noises of resistance, and the velocity fluctuation caused by minority carrier thermal motion can be equivalently expressed by the intrinsic terminal current noises [26][30]. Fig. 2.1 shows the thermal noise sources of resistances at base, emitter and collector terminals respectively as well as the terminal current noises of base and collector.

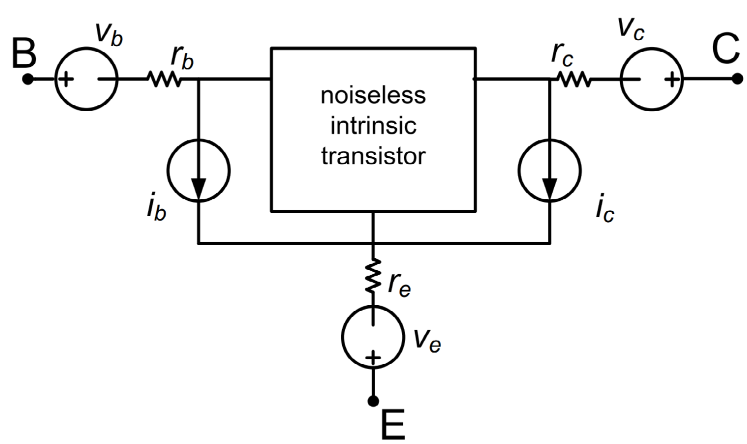

Figure 2.1: RF noise sources of a transistor.

2.1 Thermal Noise

As described by the Nyquist theorem, the power spectral density (PSD) of thermal noise voltage source of a resistance R is usually given by

$$S_{vr,vr^*} = 4KTR, \tag{2.1}$$

and the PSD of thermal noise current source is

$$S_{ir,ir^*} = \frac{4KT}{R}, \tag{2.2}$$

where K is the Boltzmann constant and T is the standardized noise source temperature 290 K.

2.2 Terminal Current Noise

2.2.1 SPICE Noise Model

The base and collector terminal noises are defined as shot noise with the PSDs,

$$\begin{cases} S_{i_c,i_{c^*}} = 2qI_C, \\ S_{i_b,i_{b^*}} = 2qI_B, \\ S_{i_c,i_{b^*}} = 0, \end{cases} \tag{2.3}$$

where I_B and I_C are base and collector DC currents.

2.2.2 Correlation Noise Model

Considering various noise physics mechanisms, a correlation noise model was developed in [8]. Fig. 2.2 illustrates the model including terminal current noises due to minority carrier velocity fluctuation and due to additional noises from the collector-base space charge region (CB SCR) transport effect. i_{b1} is the base noise current resulting from minority hole velocity fluctuation at emitter, with a PSD of $2qI_B$. i_{c1} is the collector noise current resulting from minority electron velocity fluctuation at base, with a PSD of $2qI_C$. Both of them are independent with frequency

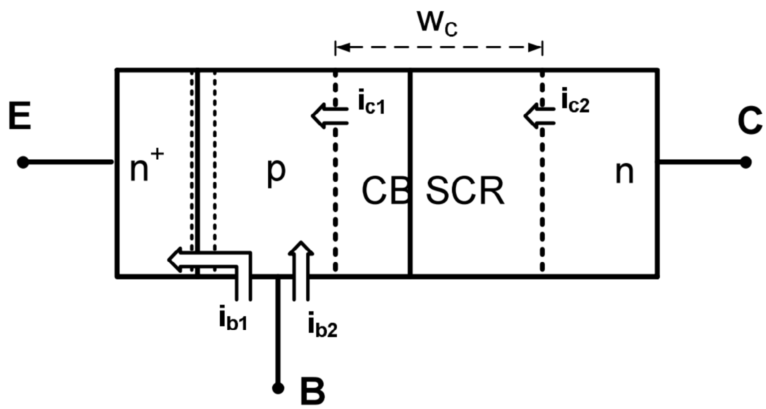

Figure 2.2: 1-D bipolar transistor with collector-base space charge region (CB SCR) effect [8].

and uncorrelated with each other. i_{c1} noise current transfer through the CB SCR becomes i_{c2} and leads to an extra base current noise i_{b2}=i_{c1}-i_{c2}.

Through a series of derivation, the final PSDs of correlation model are [8]:

$$\begin{cases} S_{i_{c2},i_{c2^*}} = 2qI_C, \\ S_{i_{b2},i_{b2^*}} = 2qI_B + 2qI_C\omega^2\tau_n^2, \\ S_{i_{c2},i_{b2^*}} = -j2qI_C\omega\tau_n, \end{cases} \tag{2.4}$$

where ω=$2\pi f$, τ_n is noise transit time which approximately equals to collector transit time [23][8].

Fig. 2.3 shows calculated PSDs of i_b and i_c versus frequency using correlation and SPICE model. It illustrates that PSDs of i_b and i_c using SPICE model are constant over frequency, while correlation leads to S_{ibib^*} increase with frequency, and imaginary part of S_{icib^*} decrease with frequency.

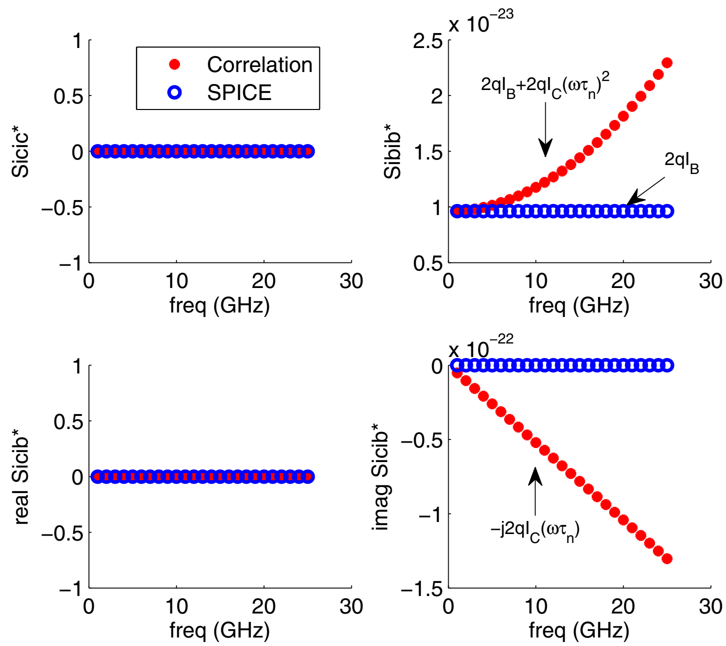

Figure 2.3: PSD of i_b and i_c using correlation model and SPICE model versus Frequency, J_C=0.414 mA/μm^2, τ_n=0.651E-12 sec, f_T=50GHz.

Chapter 3

Analytical Derivation of Noise Parameters

To obtain insight into device and LNA noise performance for design and optimization, analytical expressions of noise parameters are required. We develope analytical expressions of noise parameters for the LNA in Fig. 1.1. Z_s is source impedance that consists of resistance R_s and reactance X_s. In general, R_s=50 Ω and X_s=0 Ω. However, to examine how close noise matching is to impedance matching, we need to include X_s in Z_s to find optimal noise reactance X_{opt}. For general applicability, arbitrary L_e and L_b are used. Setting L_b=0 and L_e=0 leads to noise parameters of the transistor.

3.1 Noise Parameters of LNA

Fig. 3.1 shows a small signal equivalent circuit of Fig. 1.1. Base-collector capacitance C_{bc} and r_π between base and emitter are neglected for simplicity. This circuit includes two main kinds of RF noise sources of bipolar transistor pointed in the previous chapter, e.g. the terminal resistance thermal noise and the intrinsic terminal current noise. v_{Rs} and v_{rb} are thermal noise voltage sources due to R_s and r_b, respectively. i_b and i_c are intrinsic terminal current noise sources due to base current and collector current, respectively. C_{be} is capacitance between base and emitter. g_m is transconductance. i_{out} is output noise current due to all noise sources: v_{Rs}, v_{rb}, i_b, and i_c.

LNA noise factor, F^{LNA}, is given by:

$$F^{LNA} = 1 + \frac{Noise\ output\ due\ to\ LNA}{Noise\ output\ due\ to\ source} \tag{3.1}$$

The LNA has noise sources including the thermal noise source v_{rb} due to r_b, and the terminal noise currents i_b and i_c. The power source has a noise source v_{Rs} whose source impedance is Z_s.

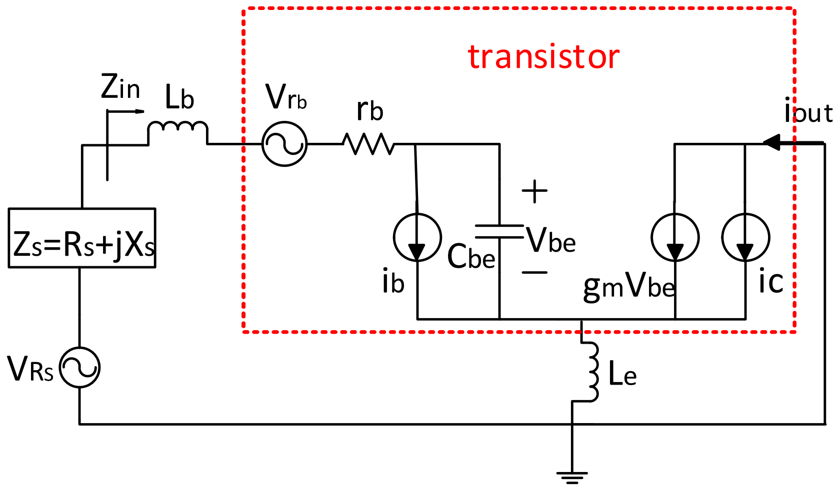

Figure 3.1: Simplified small signal equivalent circuit of LNA.

The noise currents i_b and i_c are assumed to be correlated with each other, and no correlation is a special condition when $i_b i_c^*$ and $i_c i_b^*$ terms are zero. The thermal noise v_b is independent to i_b and i_c. Therefore, (3.1) is rewritten as:

$$F^{LNA} = 1 + \frac{\left\langle \left(i_{out}^{ic} + i_{out}^{ib}\right), \left(i_{out}^{ic} + i_{out}^{ib}\right)^* \right\rangle + \left\langle i_{out}^{rb}, i_{out}^{rb*} \right\rangle}{\left\langle i_{out}^{Rs}, i_{out}^{Rs*} \right\rangle}, \tag{3.2}$$

$$\alpha = 1 - \omega^2 C_{be}(L_b + L_e) + j\omega C_{be}(Z_s + r_b) + j\omega g_m L_e, \tag{3.3}$$

$$i_{out}^{c} = V_{be}^{c} \cdot g_m + i_c = -j\omega g_m i_c L_e \cdot \frac{1}{\alpha} + i_c, \tag{3.4}$$

$$i_{out}^{b} = V_{be}^{b} \cdot g_m = -g_m i_b \left[(Z_s + r_b) + j\omega(L_b + L_e)\right] \cdot \frac{1}{\alpha}, \tag{3.5}$$

$$i_{out}^{rb} = V_{be}^{rb} \cdot g_m = -g_m v_{rb} \cdot \frac{1}{\alpha}, \tag{3.6}$$

$$i_{out}^{Rs} = V_{be}^{Rs} \cdot g_m = g_m v_{Rs} \cdot \frac{1}{\alpha}, \tag{3.7}$$

where i_{out}^{ic}, i_{out}^{ib}, i_{out}^{rb}, and i_{out}^{Rs} are output noise currents due to i_c, i_b, r_b (v_{rb}), and R_s (v_{Rs}), respectively, and can be obtained using circuit analysis. The detailed analysis is discussed in Appendix A. Noise figure NF relates to noise factor F by NF=10log F.

The output noise power produced by i_c and i_b is:

$$
\begin{aligned}
\left\langle \left(i_{out}^{ic} + i_{out}^{ib}\right), \left(i_{out}^{ic} + i_{out}^{ib}\right)^{*} \right\rangle = {} & D \left\langle ic, ic^{*} \right\rangle (\omega C_{be})^{2} |Z_s + r_b|^{2} \\
& + D \left\langle ib, ib^{*} \right\rangle g_m^{2} \left[(R_s + r_b)^{2} + (X_s + \frac{1}{\omega C_{be}})^{2} \right] \\
& - D \left\langle ic, ib^{*} \right\rangle g_m \omega C_{be} \left[(Z_s + r_b)^{*} - \frac{j}{\omega C_{be}} \right] [j(Z_s + r_b)] \\
& + D \left\langle ib, ic^{*} \right\rangle g_m \omega C_{be} \left[(Z_s + r_b) + \frac{j}{\omega C_{be}} \right] [j(Z_s + r_b)]
\end{aligned}
\tag{3.8}
$$

where

$$
D = \frac{1}{\alpha \alpha^{*}} = \frac{\frac{1}{(\omega C_{be})^{2}}}{|Z_s + r_b|^{2} + 2\omega_T L_e (R_s + r_b) + \omega_T^{2} L_e^{2}}
\tag{3.9}
$$

where $\omega_T = g_m / C_{be} = 2\pi f_T$, f_T is cut-off frequency.

$\langle ic, ic^{*} \rangle = S_{icic^{*}} \Delta f$, $\langle ib, ib^{*} \rangle = S_{ibib^{*}} \Delta f$, $\langle ic, ib^{*} \rangle = S_{icib^{*}} \Delta f$, and $\langle ib, ic^{*} \rangle = S_{ibic^{*}} \Delta f$. Δf is a very narrow bandwidth, in which the noise spectral component have a mean square value [13]. $S_{icic^{*}}$, $S_{ibib^{*}}$, $S_{icib^{*}}$, and $S_{ibic^{*}}$ are PSDs of i_b and i_c. Substituting $\langle ic, ic^{*} \rangle$, $\langle ib, ib^{*} \rangle$, $\langle ic, ib^{*} \rangle$, and $\langle ib, ic^{*} \rangle$ into (3.8):

$$
\begin{aligned}
\left\langle \left(i_{out}^{ic} + i_{out}^{ib}\right), \left(i_{out}^{ic} + i_{out}^{ib}\right)^{*} \right\rangle = {} & D S_{icic^{*}} \Delta f (\omega C_{be})^{2} |Z_s + r_b|^{2} \\
& + D S_{ibib^{*}} \Delta f g_m^{2} \left[(R_s + r_b)^{2} + (X_s + \frac{1}{\omega C_{be}})^{2} \right] \\
& - D 2 g_m \Delta f \Re(S_{icib^{*}}) (R_s + r_b) \\
& + D 2 g_m \Delta f \Im(S_{icib^{*}}) \left[\omega C_{be} |Z_s + r_b|^{2} + X_s \right],
\end{aligned}
\tag{3.10}
$$

where $\Re$ stands for real part, and $\Im$ stands for imaginary part.

The output noise power produced by r_b is:

$$
\left\langle i_{out}^{ib}, i_{out}^{ib*} \right\rangle = g_m^{2} D 4 k T r_b \Delta f,
\tag{3.11}
$$

where k is Boltzmann constant, and T is temperature, which is assumed to be equal to standardized noise source temperature 290 K here for simplicity.

The output noise power produced by R_s is:

$$
\left\langle i_{out}^{R_s}, i_{out}^{R_s *} \right\rangle = g_m^{2} D 4 k T R_s \Delta f.
\tag{3.12}
$$

Substituting (3.10), (3.11), and (3.12) into (3.2), we get noise figure of an LNA:

$$
\begin{aligned}
F^{LNA} =& 1+\frac{r_b}{R_s} \\
&+\frac{S_{icic^*}}{4kTR_s}\left(\frac{\omega}{\omega_T}\right)^2\left[\left(\frac{\omega_T}{\omega g_m}-\ell\right)^2+(R_s+r_b)^2\right] \\
&+\frac{S_{ibib^*}}{4kTR_s}\left[(R_s+r_b)^2+\ell^2\right] \\
&-\frac{\Re(S_{icib^*})}{2g_mkTR_s}(R_s+r_b) \\
&+\frac{\Im(S_{icib^*})}{2kTR_s}\left(\frac{\omega}{\omega_T}\right)\left[(R_s+r_b)^2-\ell\left(\frac{\omega_T}{\omega g_m}-\ell\right)\right],
\end{aligned}
\tag{3.13}
$$

where ℓ=X_s+$\omega(L_b+L_e)$. In both SPICE model and correlation model, $\Re(S_{icib^*})$=0, thus we set $\Re(S_{icib^*})$=0 in below.

To find out the optimum X_s, X_{opt}^{LNA} to minimize the noise figure, we solve $\partial F^{LNA}/\partial X_s=0$:

$$
\begin{aligned}
\frac{\partial F^{LNA}}{\partial X_s} =& -\frac{S_{icic^*}}{2kTR_s}\left(\frac{\omega}{\omega_T}\right)^2\left(\frac{\omega_T}{\omega g_m}-\ell\right) \\
&+\frac{S_{ibib^*}}{2kTR_s}\ell-\frac{\Im(S_{icib^*})}{skTR_s}\left(\frac{\omega}{\omega_T}\right)\left(\frac{\omega_T}{\omega g_m}-2\ell\right)=0,
\end{aligned}
\tag{3.14}
$$

$$
\ell\left[S_{ibib^*}+S_{icic^*}\left(\frac{\omega}{\omega_T}\right)^2+2\Im(S_{ibib^*})\left(\frac{\omega}{\omega_T}\right)\right]+S_{icic^*}\left(\frac{\omega}{\omega_T g_m}\right)-\frac{\Im(S_{icib^*})}{g_m}=0, \tag{3.15}
$$

where ω_T=g_m/C_{be}. Substituting ℓ=X_s+$\omega(L_b+L_e)$ in (3.15), we obtain the expression of X_{opt}^{LNA}:

$$
X_{opt}^{LNA} = \frac{1}{N}\frac{\omega_T}{g_m\omega}\left[S_{icic^*}+\Im(S_{icib^*})\left(\frac{\omega_T}{\omega}\right)\right]-\omega(L_b+L_e), \tag{3.16}
$$

where

$$
N = S_{icic^*}+S_{ibib^*}\left(\frac{\omega_T}{\omega}\right)^2+2\Im(S_{icib^*})\left(\frac{\omega_T}{\omega}\right). \tag{3.17}
$$

To find the optimum R_s that minimizes F^{LNA}, R_{opt}^{LNA}, we solve $\partial F^{LNA}/\partial R_s=0$. The result is:

$$
R_{opt}^{LNA} = \frac{\sqrt{A}}{N}, \tag{3.18}
$$

$$A = r_b^2 N^2 + \underbrace{\left(\frac{\omega_T}{\omega}\right)^2 4kTr_bN}_{v_{rb}\text{ contribution}} + \frac{1}{g_m^2}\left(\frac{\omega_T}{\omega}\right)^4 \left(S_{icic^*}S_{ibib^*} - \Im(S_{icib^*})^2\right), \tag{3.19}$$

Substituting (3.16) and (3.18) into (3.13) leads to the minimum noise factor of LNA, F_{min}^{LNA}:

$$F_{min}^{LNA} = 1 + \underbrace{\frac{r_b}{R_{opt}^{LNA}}}_{v_{rb}\text{ contribution}} + \frac{\left(R_{opt}^{LNA} + r_b\right)^2}{4kTR_{opt}^{LNA}}\left(\frac{\omega}{\omega_T}\right)^2 N + \frac{1}{4kTR_{opt}^{LNA}}\frac{1}{g_m^2}\left(\frac{\omega_T}{\omega}\right)^2 \frac{\left(S_{icic^*}S_{ibib^*} - \Im(S_{icib^*})^2\right)}{N}, \tag{3.20}$$

where the r_b/R_{opt}^{LNA} term is due to v_{rb} which represents the effect of r_b as a noise source. The remaining terms of (3.20) are due to i_c, i_b, and v_{Rs}, and depend on r_b because r_b affects how i_c, i_b, and v_{Rs} are transferred to i_{out}. Here r_b's effect is manifested as an impedance element. While r_b as a noise source is generally understood to be important, r_b as an impedance element is much more important in affecting F_{min}, as detailed below in Chapter 4.

Noise resistance R_n^{LNA} could be obtained the following equation which is from linear noisy two-port theory [13][31]:

$$R_n = \frac{S_{v_a,v_a^*}}{4KT}, \tag{3.21}$$

where S_{v_a,v_a^*} is chain representation equivalent input noise voltage [26][31], and could be calculated by:

$$S_{v_a,v_a^*} = \frac{\left\langle i_{out}, i_{out}^* \right\rangle_{Rn}}{|Y_{21}|^2}, \tag{3.22}$$

where Y_{21} is the forward transfer admittance with output short circuit, and $\left\langle i_{out}, i_{out}^* \right\rangle_{Rn}$ is the total output noise power without power source, as shown in Fig. 3.2:

$$\left\langle i_{out}, i_{out}^* \right\rangle_{Rn} = \left\langle (i_{out,Rn}^{ic} + i_{out,Rn}^{ib}), (i_{out,Rn}^{ic} + i_{out,Rn}^{ib})^* \right\rangle_{Rn} + \left\langle i_{out,Rn}^{r_b}, i_{out,Rn}^{r_b *} \right\rangle. \tag{3.23}$$

We find out $i_{out,Rn}^{ic}$, $i_{out,Rn}^{ib}$,$i_{out,Rn}^{r_b}$ using equivalent circuit in Fig. 3.2:

$$\alpha_{Rn} = 1 - \omega^2 C_{be}(L_b + L_e) + j\omega C_{be} r_b + j\omega g_m L_e, \tag{3.24}$$

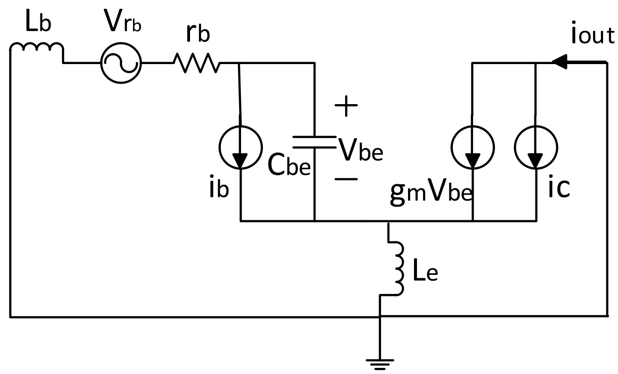

Figure 3.2: Equivalent circuit of simplified LNA without power source.

$$i^{c}_{out,Rn} = \frac{i_c}{\alpha_{Rn}}\left[1-\omega^2 C_{be}(L_e+L_b)+j\omega C_{be} r_b\right], \tag{3.25}$$

$$i^{b}_{out,Rn} = -\frac{g_m i_b}{\alpha_{Rn}}\left[r_b + j\omega(L_b+L_e)\right], \tag{3.26}$$

$$i^{rb}_{out,Rn} = -\frac{g_m v_{rb}}{\alpha_{Rn}}. \tag{3.27}$$

The output noise power produced by i_c and i_b is:

$$\begin{aligned}
&\left\langle (i^{ic}_{out}+i^{ib}_{out}),(i^{ic}_{out}+i^{ib*}_{out})\right\rangle_{Rn} \\
&= D_{Rn}\langle ic, ic^*\rangle\left[\left(1-\omega^2 C_{be}\left(L_e+L_b\right)\right)^2+\omega^2 C_{be}^2 r_b^2\right] \\
&+ D_{Rn}\langle ib, ib^*\rangle g_m^2\left[r_b^2+\omega^2\left(L_e+L_b\right)^2\right] \\
&- 2D_{Rn}\Delta f\Re(S_{icib^*})g_m r_b \\
&+ 2D_{Rn}\Delta f\Im(S_{icib^*})g_m\left[-\omega C_{be} r_b^2+\omega\left(L_e+L_b\right)\left(1-\omega^2 C_{be}\left(L_e+L_b\right)\right)\right],
\end{aligned} \tag{3.28}$$

where D_{Rn} is:

$$D_{Rn} = \frac{1}{\left[1-\omega^2 C_{be}\left(L_e+L_b\right)\right]^2+\omega^2\left(C_{be} r_b+g_m L_e\right)^2}. \tag{3.29}$$

The output noise power produced by r_b is:

$$\left\langle i^{r_b}_{out}, i^{r_b*}_{out}\right\rangle = g_m^2 D_{Rn} * 4kTr_b\Delta f. \tag{3.30}$$

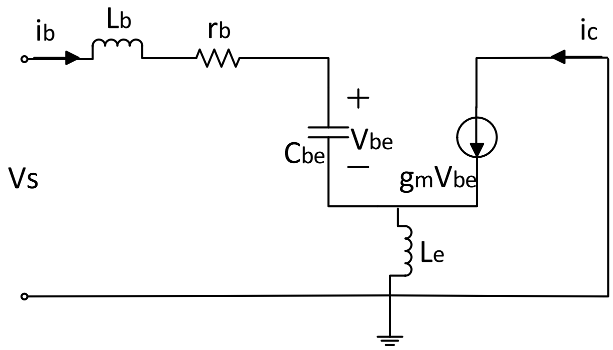

Figure 3.3: Equivalent small signal circuit of simplified LNA without noise sources.

Y_{21} is calculated using Fig. 3.3:

$$Y_{21} = \frac{i_{out}}{V_s} = \frac{i_c}{r_b i_c + V_{be} + j\omega L_b i_b + j\omega(i_b + i_c)L_e}, \tag{3.31}$$

$$\frac{1}{Y_{21}} = \frac{r_b}{\beta_{RF}} + \frac{1}{g_m} + \frac{j\omega}{\beta_{RF}}(L_b + L_e) + j\omega L_e, \tag{3.32}$$

where $\beta_{RF} = \frac{g_m}{j\omega C_{be}} = \frac{\omega_T}{j\omega}$. Therefore,

$$\begin{aligned}\frac{1}{|Y_{21}|^2} &= \left[\frac{1}{g_m} - \frac{\omega^2}{\omega_T}(L_b + L_e)\right]^2 + \left(r_b \frac{\omega}{\omega_T} + \omega L_e\right)^2 \\ &= \frac{1}{g_m}\left[\left[1 - \omega^2 C_{be}(L_e + L_b)\right]^2 + \omega^2 (C_{be} r_b + g_m L_e)^2\right] \\ &= \frac{1}{g_m^2 D_{Rn}}.\end{aligned} \tag{3.33}$$

From (3.21)-(3.33), we obtain the noise resistance of LNA, R_n^{LNA}:

$$\begin{aligned}R_n^{LNA} =& r_b + \frac{r_b^2 + \omega^2 (L_e + L_b)^2}{4KT} S_{ibib^*} \\ &+ \frac{\left[1 - \omega^2 C_{be}(L_e + L_b)\right]^2 + \omega^2 C_{be}^2 r_b^2}{4KT g_m^2} S_{icic^*} \\ &+ \frac{r_b}{2KT g_m} \Re(S_{icib^*}) \\ &+ \frac{\omega C_{be} r_b^2 - \omega (L_e + L_b)\left(1 - \omega^2 C_{be}(L_e + L_b)\right)}{2KT g_m} \Im(S_{icib^*}).\end{aligned} \tag{3.34}$$

Setting $\Re(S_{icib^*})$=0 in (3.34), the noise resistance of LNA is:

$$\begin{aligned} R_n^{LNA} =& r_b + \frac{r_b^2 + \omega^2 (L_e + L_b)^2}{4KT} S_{ibib^*} \\ &+ \frac{\left[1 - \omega^2 C_{be} (L_e + L_b)\right]^2 + \omega^2 C_{be}^2 r_b^2}{4KTg_m^2} S_{icic^*} \\ &+ \frac{\omega C_{be} r_b^2 - \omega (L_e + L_b)\left(1 - \omega^2 C_{be} (L_e + L_b)\right)}{2KTg_m} \Im(S_{icib^*}). \end{aligned} \tag{3.35}$$

3.2 Device Noise Parameters and Relations to LNA Noise Parameters

An inspection of (3.16), (3.18), and (3.20) shows that L_b and L_e only enter (3.16), expression of X_{opt}^{LNA}, and 3.35, expression of R_n^{LNA}. Therefore, transistor R_{opt} and F_{min} are as the same as LNA R_{opt} and F_{min}:

$$R_{opt}^{Device} = R_{opt}^{LNA}, \tag{3.36}$$

$$F_{min}^{Device} = F_{min}^{LNA}. \tag{3.37}$$

Setting L_b and L_e to zero in (3.16), we obtain transistor X_{opt}^{Device}:

$$\begin{aligned} X_{opt}^{Device} &= X_{opt}^{LNA} + \omega (L_b + L_e) \\ &= \frac{1}{N} \frac{\omega_T}{\omega g_m} \left[S_{icic^*} + \Im(S_{icib^*}) \left(\frac{\omega_T}{\omega} \right) \right]. \end{aligned} \tag{3.38}$$

Setting L_b and L_e zero in (3.35), we obtain noise resistance of device R_n^{Device}:

$$R_n^{Device} = r_b + \frac{r_b^2}{4KT} S_{ibib^*} + \left[\frac{1}{4KTg_m^2} + \frac{\left(\frac{\omega}{\omega_T}\right)^2 r_b^2}{4KT} \right] S_{icic^*} + \frac{\left(\frac{\omega}{\omega_T}\right) r_b^2}{2KT} \Im(S_{icib^*}). \tag{3.39}$$

These relations between device and LNA noise parameters can also be obtained using two-port combining techniques [13][31], and hold with or without correlation.

Chapter 4

Impact of Correlation on Device Noise Parameters

In the SPICE model, i_b and i_c noise currents are described as shot noise of majority carriers passing through the EB and CB junction, which relate to the corresponding DC currents by $2qI$. At higher frequency, i_b increases with frequency and is correlated with i_c, due to both base and CB SCR transport, with the later dominant in modern HBTs [23]. For analytical analysis, we use the correlation model in [8]. Table 4.1 shows S_{ibib^*}, S_{icic^*}, S_{icib^*}, and S_{ibic^*} of correlation model in [8] and SPICE noise model. τ_n is noise transit time which approximately equals to collector transit time [23][8]. Substituting expressions of S_{ibib^*}, S_{icic^*}, and $\Im(S_{icib^*})$ into (3.36), (3.37), (3.38), and (3.39), we obtain device noise parameters with and without correlation, i.e. the SPICE model.

Table 4.1: S_{ibib^*}, S_{icic^*}, S_{icib^*}, and S_{ibic^*} of Correlation model and SPICE model

	SPICE	Correlation
S_{icic^*}	$2qI_C$	$2qI_C$
S_{ibib^*}	$2qI_B$	$2qI_B + 2qI_C(\omega\tau_n)^2$
S_{icib^*}	0	$-j2qI_C(\omega\tau_n)$
S_{ibic^*}	0	$j2qI_C(\omega\tau_n)$

4.1 Analytical Model Verification

Fig. 4.1 compares analytical model, Agilent ADS simulation and measurement of F_{min}^{Device}, R_{opt}^{Device}, and X_{opt}^{Device} versus J_C at 5 GHz. The device used is from a commercial SiGe HBT BiCMOS technology, with an emitter area A_E of 0.8×20×3 μm^2, a peak f_T of 36 GHz, and a peak f_{max} of 65 GHz. Measurement data were obtained using a commercial system, and have been de-embedded. A modified HICUM model with correlation is used [8]. τ_n is extracted by fitting measured noise parameters [19]. Other compact model parameters are extracted by fitting

DC I-V curves and Y-parameters. For calculation, i_b, i_c, r_b, g_m, ω_T, and τ_n are generated from operation point information using the *ddx* operator in the Verilog-A device model. The Matlab codes for noise parameters calculation are shown in Appendix B.

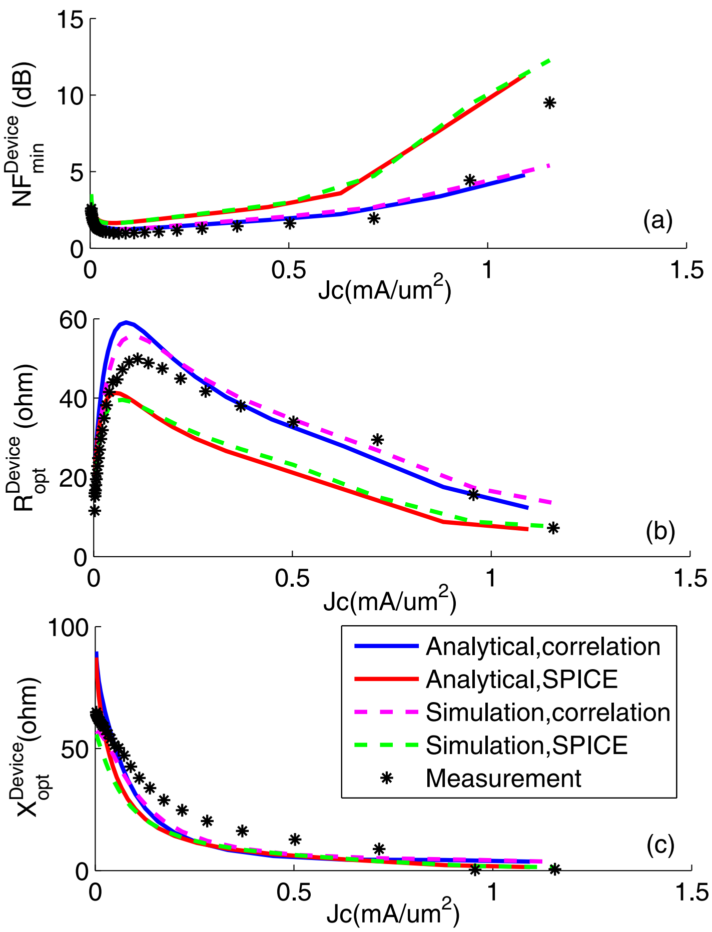

Figure 4.1: Analytical, simulated and measured noise parameters of SiGe HBT with A_E=0.8×20×3 μm^2 versus J_C at V_{CE}=3.3 V, f=5 GHz.

Analytical model agrees fairly well with simulation. Correlation model is much closer to measured data than SPICE [10], especially at higher J_C. Correlation leads to smaller NF_{min} and larger R_{opt} as detailed below.

4.2 Correlation's Impact on R_{opt}^{Device}

Since emitter length is first decided in LNA design for R_{opt}^{Device}=50 Ω, and NF_{min} requires R_{opt}, we discuss the impact of correlation on R_{opt}^{Device} first. In Fig. 4.1 (b), the R_{opt}^{Device} with correlation is larger. To see if this can be generalized, we further simplify R_{opt}^{Device} by substituting expressions of PSDs from Table 4.1 into (3.36), and approximating g_m with $(qI_C)/(kT)$. The N in (3.17) can be rewritten as $2qI_cM$, with M being:

$$M = \begin{cases} M_{Spice} = 1 + \frac{1}{\beta}\left(\frac{\omega_T}{\omega}\right)^2, & \text{SPICE} \\ M_{Cor} = 1 + \frac{1}{\beta}\left(\frac{\omega_T}{\omega}\right)^2 + (\omega_T\tau_n)^2 - \omega_T\tau_n, & \text{Correlation} \end{cases} \tag{4.1}$$

where β=I_C/I_B, M_{Spice} and M_{Cor} are M for SPICE model and correlation model. Then,

$$R_{opt}^{Device} = \sqrt{r_b^2 + \left(\frac{\omega_T}{\omega}\right)^2 \left[\underbrace{\frac{2r_b}{g_m M}}_{v_{rb}\text{ contribution}} + \frac{1}{M^2}\frac{1}{g_m^2\beta}\left(\frac{\omega_T}{\omega}\right)^2 \right]}. \tag{4.2}$$

(4.2) shows that the only difference between R_{opt}^{Device} with and without correlation is factor M. As f_T<$1/(2\pi\tau_f)$, and τ_n<τ_f, with τ_f being the forward transit time, $\omega_T\tau_n$<1. In M_{cor}, $(\omega_T\tau_n)^2$-$\omega_T\tau_n$<0, thus M_{cor}<M_{Spice}. M appeared in (4.2) as "$1/M$", thus correlation noise leads to a larger R_{opt} for given emitter length.

r_b shows up in two places in (4.2). An inspection of the derivation details shows that term $2r_b/(g_mM)$ is due to v_{rb}, and term r_b^2 is due to r_b as an impedance. $2r_b/(g_mM)$ shows that r_b as noise source influences the weight of M in R_{opt}^{Device}, and then the impact of correlation on R_{opt}^{Device}. Roles of r_b will be further discussed in section 4.6.

4.3 Correlation's Impact on F_{min}^{Device}

In Fig. 4.1 (a), NF_{min}^{Device} using correlation model is smaller than NF_{min}^{Device} using SPICE model, especially at higher J_C. Substituting expressions of S_{ibib^*}, S_{icic^*}, and $\Im(S_{icib^*})$ from Table

4.1 into (3.37) and using $g_m \approx (qI_C)/(kT)$ lead to simplified F_{min}^{Device}:

$$\begin{aligned} F_{min}^{Device} = 1 + & \underbrace{\frac{r_b}{R_{opt}^{Device}}}_{v_{rb} \text{ contribution}} \\ & + \frac{g_m}{2}\left(\frac{\omega}{\omega_T}\right)^2 \left(1 + \frac{r_b}{R_{opt}^{Device}}\right)^2 R_{opt}^{Device} M \\ & + \frac{1}{2g_m\beta}\frac{1}{R_{opt}^{Device}}\left(\frac{\omega_T}{\omega}\right)^2 \frac{1}{M}. \end{aligned} \tag{4.3}$$

Difference between F_{min}^{Device} with and without correlation lies in M and R_{opt}^{Device}. The last term in (4.3) is small and negligible. Since $R_{opt,cor}^{Device} > R_{opt,Spice}^{Device}$, the second term r_b/R_{opt}^{Device} is smaller with correlation. Since $M_{cor}R_{opt,cor}^{Device} < M_{Spice}R_{opt,Spice}^{Device}$ in the third term, correlation noise leads to a smaller F_{min}^{Device}.

4.4 Correlation's Impact on X_{opt}^{Device}

Substituting expressions of $S_{i_b i_b^*}$, $S_{i_c i_c^*}$, and $\Im(S_{i_c i_b^*})$ from Table 4.1 into (3.38) leads to X_{opt}^{Device} with and without correlation, $X_{opt,Spice}^{Device}$ and $X_{opt,cor}^{Device}$:

$$X_{opt,Spice}^{Device} = \frac{1}{g_m}\frac{\omega_T}{\omega}\frac{1}{1 + \frac{1}{\beta}\left(\frac{\omega_T}{\omega}\right)^2}, \tag{4.4}$$

$$X_{opt,cor}^{Device} = \frac{1}{g_m}\frac{\omega_T}{\omega}\frac{1 - \omega_T\tau_n}{1 + \frac{1}{\beta}\left(\frac{\omega_T}{\omega}\right)^2 - \omega_T\tau_n\left(2 - \omega_T\tau_n\right)}, \tag{4.5}$$

where $\omega_T\tau_n < 1$, thus $\omega_T\tau_n$ is smaller than $\omega_T\tau_n(2\text{-}\omega_T\tau_n)$ in $X_{opt,cor}^{Device}$. Therefore, correlation results in an increase in X_{opt}^{Device}. Observe that X_{opt}^{Device} remains positive with correlation, indicating an inductive source is required.

4.5 Correlation's Impact on R_n^{Device}

Substituting expressions of S_{ibib^*}, S_{icic^*}, and $\Im(S_{icib^*})$ from Table 4.1 into (3.39) leads to R_n^{Device} with and without correlation, $R_{n,Spice}^{Device}$ and $R_{n,cor}^{Device}$:

$$R_{n,Spice}^{Device} = r_b + \frac{r_b^2 g_m}{2}\frac{1}{\beta} + \frac{1}{2g_m} + \frac{r_b^2 g_m}{2}\left(\frac{\omega}{\omega_T}\right)^2, \tag{4.6}$$

$$R_{n,cor}^{Device} = r_b + \frac{r_b^2 g_m}{2}\frac{1}{\beta} + \frac{1}{2g_m} + \frac{r_b^2 g_m}{2}\left(\frac{\omega}{\omega_T} - \omega\tau_n\right)^2. \tag{4.7}$$

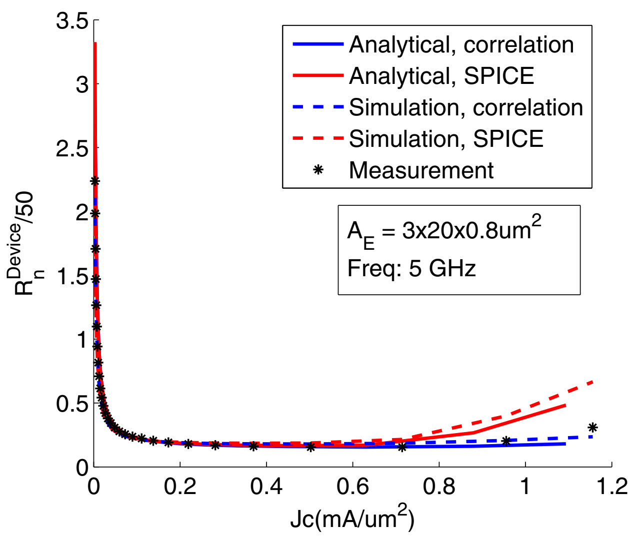

Figure 4.2: Device noise resistance R_n normalized by 50 Ω.

Fig. 4.2 shows device noise resistance normalized by 50 Ω versus J_C. Analytical models agree with simulation. $R_n/50$ with and without correlation noise are very close except at high J_C. Because of additional term $\omega\tau_n$ in (4.7), R_n with correlation is slightly smaller than that without correlation. Since τ_n increases with J_C, this difference is more obvious at higher J_C at a given frequency.

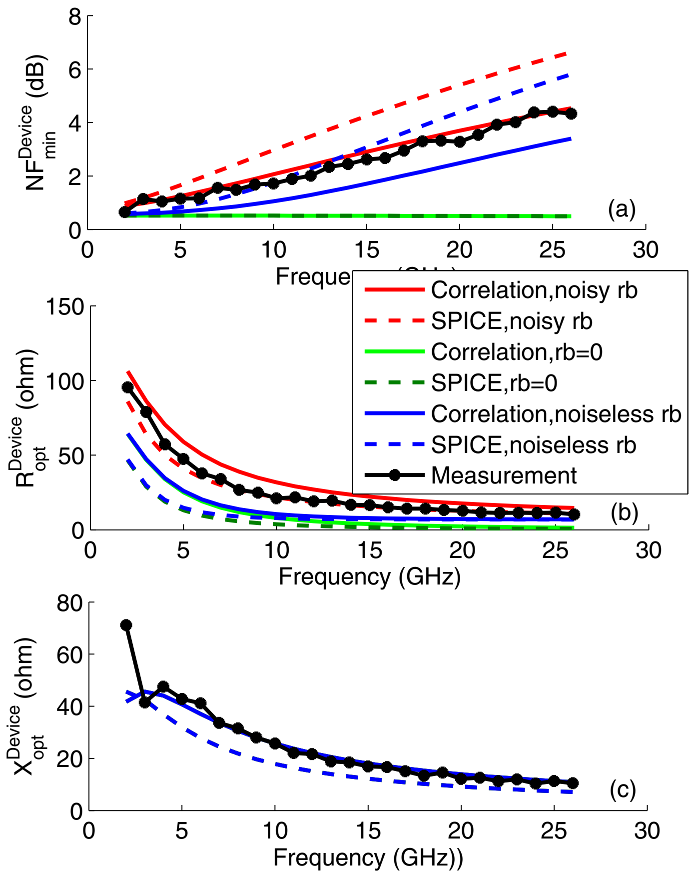

Figure 4.3: Analytical and measured noise parameters of SiGe HBT device versus frequency at V_{CE}=3.3 V, I_c=3.47 mA.

4.6 Two Roles of r_b

In (4.2) and (4.3), r_b plays two roles: 1) r_b generates thermal noise, i.e. the v_{rb} in Fig. 3.1; 2) r_b affects calculation of i_{out}^{ic}, i_{out}^{ib}, and i_{out}^{Rs} as an impedance, i.e. the r_b in Fig. 3.1. To examine the roles of r_b, we show in Fig. 4.3 F_{min}^{Device}, R_{opt}^{Device}, and X_{opt}^{Device} versus frequency at I_c=3.47mA obtained with:

1. r_b=0: all r_b in (4.2) and (4.3) are set to zero;

2. noiseless r_b: r_b only acts as an impedance; the terms $2r_b/(g_m M)$ in (4.2) and r_b/R_{opt}^{Device} in (4.3) are set to zero;

3. noisy r_b: r_b acts as both impedance and noise source.

The difference between r_b=0 and noiseless r_b curves indicates r_b's importance as impedance. The difference between noiseless r_b and noisy r_b curves indicates r_b's importance as noise source.

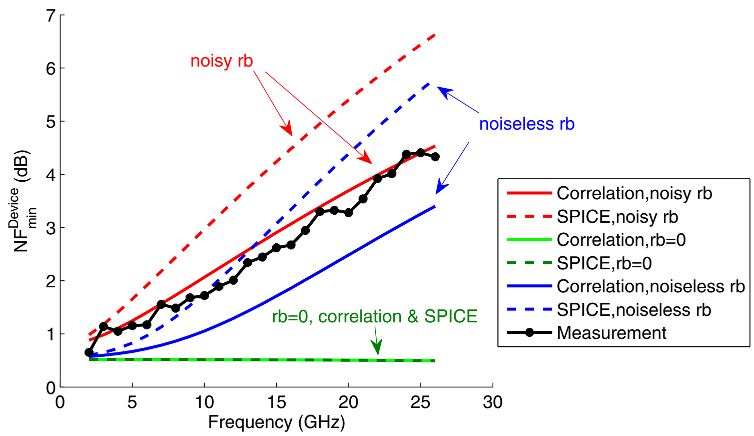

Figure 4.4: r_b's impact on NF_{min} of device versus frequency at V_{CE}=3.3 V, I_c=3.47 mA.

Fig. 4.3 shows that r_b affects NF_{min} most. From Fig. 4.4, r_b's impact on NF_{min} can be observed:

1. At r_b=0, NF_{min} with and without correlation are the same:

$$NF_{min}^{Device} = 1 + \sqrt{\frac{1}{\beta}}. \tag{4.8}$$

Therefore, the impact of correlation on NF_{min} depends on r_b. Noise correlation does not necessarily reduce NF_{min}. In addition, NF_{min} with r_b=0 is much lower than that with r_b, especially at high frequency. This suggests NF_{min} can be decreased by reducing r_b at given device size in modern technology.

2. The NF_{min} with noiseless r_b is closer to noisy r_b than to r_b=0, thus r_b as an impedance plays a much more important role than r_b as a noise source.

3. The difference between NF_{min} using SPICE model and correlation model becomes larger at higher frequency, which means the effects of r_b on noise correlation's impact are more obvious at higher frequency.

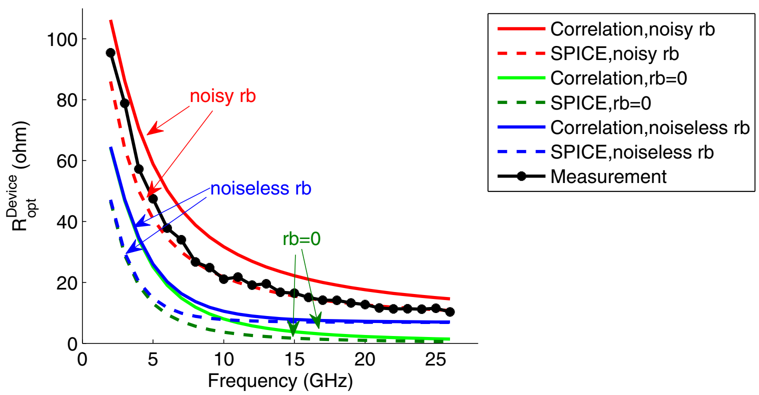

Figure 4.5: r_b's impact on R_{opt} of device versus frequency at V_{CE}=3.3 V, I_c=3.47 mA.

Fig. 4.5 shows r_b's impact on R_{opt}. R_{opt} with noiseless r_b are closer to r_b=0 than to noisy r_b, indicating that r_b as noise source plays a slightly more important role than r_b as an impedance.

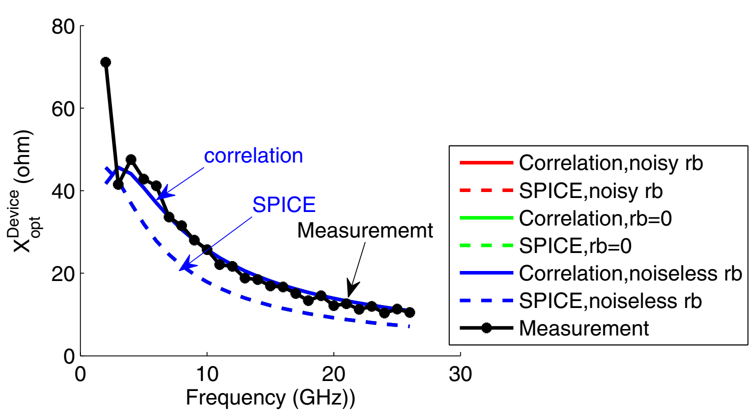

Figure 4.6: r_b's impact on X_{opt} of device versus frequency at V_{CE}=3.3 V, I_c=3.47 mA.

Fig. 4.6 shows r_b's impact on X_{opt}. Noisy r_b, r_b=0, and noiseless r_b overlay together, thus only three curves are shown: using SPICE model curve, using correlation model curve, and measurement curve. X_{opt}^{Device} is independent from r_b in (4.4) and (4.5).

4.7 Correlation and r_b Interaction

In [12][13][14][15][16][17][24][32], a very popularly used F_{min}^{Device} equation based on SPICE model was used:

$$F_{min}^{Device} = 1 + \sqrt{2g_m r_b}\sqrt{\frac{1}{\beta} + \left(\frac{f}{f_T}\right)^2}. \tag{4.9}$$

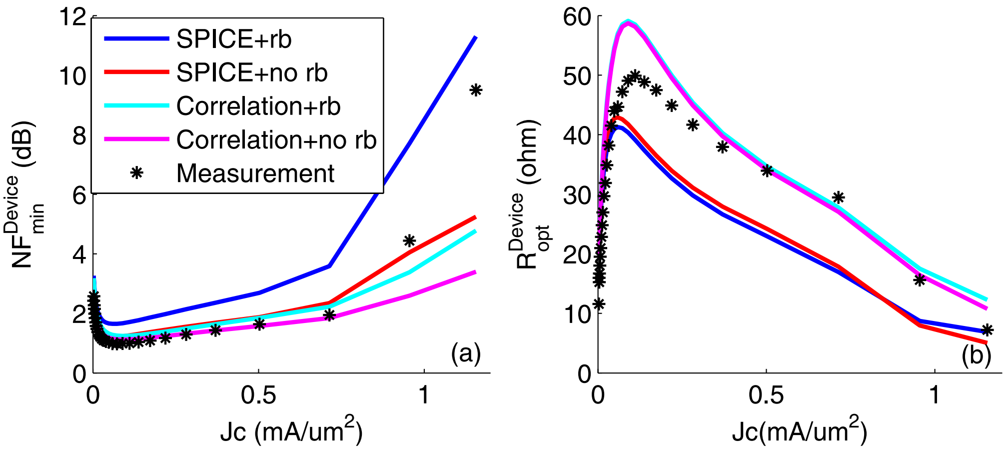

Figure 4.7: (a)NF_{min}^{Device} versus J_C at 5 GHz; (b)R_{opt}^{Device} versus J_C at 5 GHz.

A detailed analysis of its derivation shows that (4.9) also neglects r_b's role as impedance. (4.9) can be obtained from (4.3) using SPICE model, including r_b's role as noise source, but neglecting r_b's role as impedance. (4.9) is popular as it gives good agreement with measurement. The reason why (4.9) "agrees" with measurement is the opposite effects of noise correlation and r_b's role as impedance on NF_{min}, as illustrated in Fig. 4.7(a), where NF_{min}^{Device} versus J_C is calculated with and without considering r_b's role as impedance, for both SPICE and correlation models.

r_b's role as noise source is included for all curves. *"r_b"* and *"no r_b"* stand for with and without impedance r_b, respectively. Without impedance r_b, for both correlation and SPICE models, NF_{min}^{Device} is smaller. With correlation, NF_{min}^{Device} is smaller with or without impedance r_b. Correlation decreases NF_{min}^{Device}, while impedance r_b increases NF_{min}^{Device}. (4.9) does not account for correlation, and neglects impedance r_b, i.e. the *"SPICE+no r_b"*. The resulting NF_{min}^{Device}, however, is close to *"Correlation+r_b"* and measurement. This coincidence makes (4.9) seem reasonable. It is worth noting that although (4.9) agrees with measurement, it is inaccurate compared to SPICE model circuit simulations which normally include r_b's impedance role.

This coincidence, however, doesn't happen to R_{opt}^{Device}, since r_b plays less important role as impedance than as noise source in R_{opt}^{Device}. In Fig. 4.7(b), at which R_{opt}^{Device} versus J_C is calculated, R_{opt}^{Device} is close to measurement only when correlation noise is considered. In LNA design, emitter length L_E is directly decided by R_{opt}^{Device}, as detailed in chapter 5.

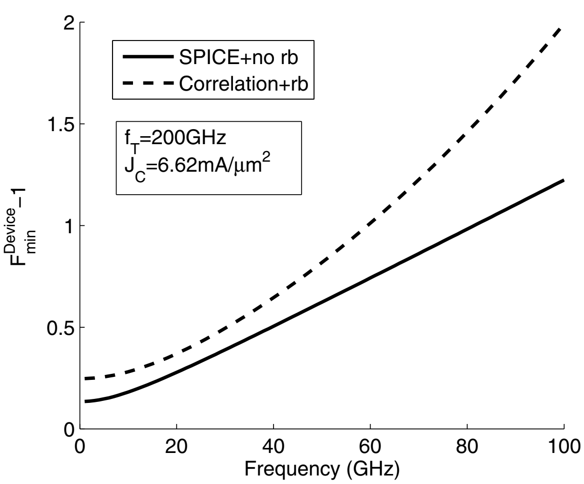

Figure 4.8: $F_{min} - 1$ versus frequency at J_C=6.62 mA/μm^2.

Another implication of (4.9) is that $F_{min} - 1$ increases with frequency linearly, and this was used to extrapolate measurement below 26GHz to 60GHz [15]. Fig. 4.8 shows $F_{min} - 1$ versus frequency. $F_{min} - 1$ is linear without r_b as an impedance. r_b's impedance role makes $F_{min} - 1$ versus frequency less linear, which predicts the noise performance more precisely.

Chapter 5

LNA Design Implication

At a fixed J_C, the following transistor scaling rules of emitter length L_E exist: $r_b \propto 1/L_E$, $I_C \propto L_E$, and $C_{be} \propto L_E$ [16][33]. Substituting them into expressions of R_{opt}^{LNA}, X_{opt}^{LNA}, and F_{min}^{LNA}, we obtain that $R_{opt}^{LNA} \propto 1/L_E$, $X_{opt}^{LNA} \propto 1/L_E$, and F_{min}^{LNA} is independent of L_E at a given J_C.

To examine how frequency dependent noise correlation affects LNA design, we design LNA using correlation model and SPICE model as following steps. At a given J_C,

1. choose L_E=$(R_{opt}^{ref} L_E^{ref})/50\Omega$, where "ref" stands for reference;

2. set L_b and L_e for input impedance matching:

$$\begin{cases} L_e = \frac{R_s - r_b}{\omega_T}, \\ L_b = \frac{1}{\omega^2 C_{be}} - \frac{R_s - r_b}{\omega_T}. \end{cases} \tag{5.1}$$

Then we will examine how correlation affects X_{opt}^{LNA}, which is supposed to approximately be zero using SPICE model [12][24].

Fig. 5.1 shows analytical R_{opt}^{LNA}, X_{opt}^{LNA}, NF_{min}^{LNA}, and NF^{LNA} of impedance matched LNA versus L_E at J_C=0.158mA/μm^2, f=5GHz. R_{opt}^{LNA}, X_{opt}^{LNA}, and NF_{min}^{LNA} are plotted by substituting (5.1) into (3.16), (3.18), and (3.20) that impedance matches at each L_E. NF^{LNA} are plotted by setting R_s=50Ω and X_s=0 in (3.13). The markers on R_{opt}^{LNA} curves are firstly decided at L_E required for R_{opt}^{LNA}=50Ω. Then X_{opt}^{LNA}, NF_{min}^{LNA}, and I_C at corresponding L_E are also marked.

At L_E required for R_{opt}^{LNA}=50 Ω, X_{opt}^{LNA} equals to -2.924 Ω for correlation model and -8.286 Ω for SPICE model. The closeness between X_{opt}^{LNA} and zero is better with correlation. Even though X_{opt}^{LNA} slightly deviates from zero, NF^{LNA} is very close to NF_{min}^{LNA}. Also, noise

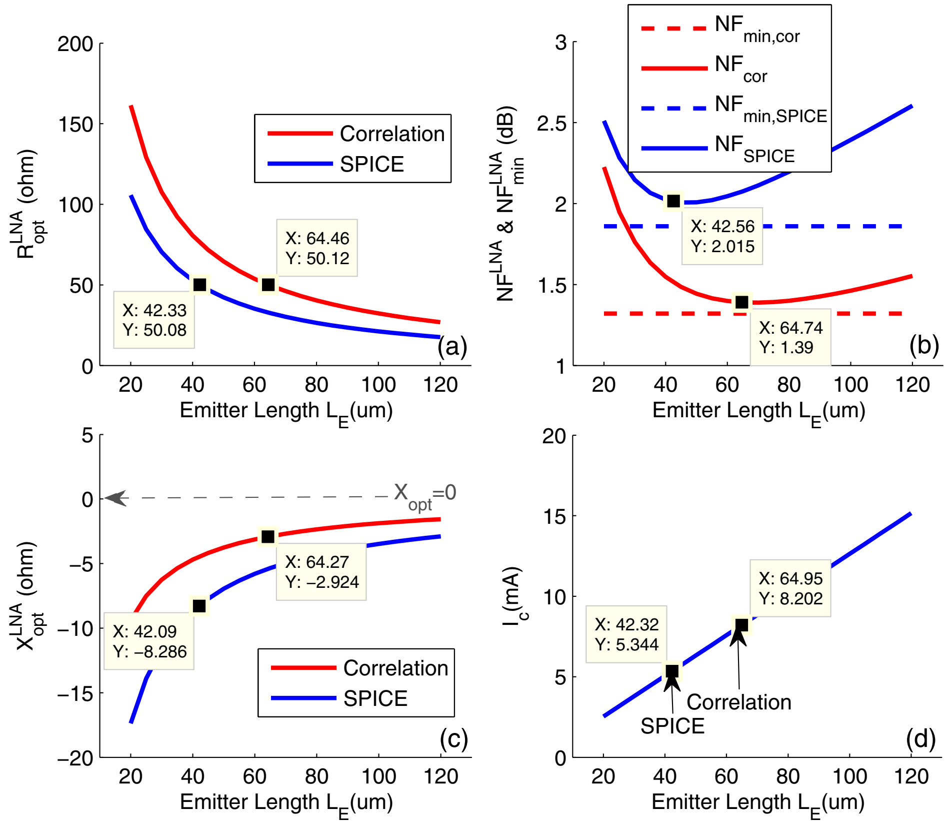

Figure 5.1: R_{opt}^{LNA}, X_{opt}^{LNA}, NF_{min}^{LNA}, and NF^{LNA} of impedance matched LNA versus L_E at J_C=0.158 mA/μm^2, f=5 GHz

correlation provides smaller distance between NF^{LNA} and NF_{min}^{LNA}. In this case, correlation leads to more closeness between noise and impedance matching.

A larger L_E required using correlation model results in a higher I_C: 8.202mA for correlation model versus 5.344mA for SPICE model. To constrain power consumption, L_E does not have to be chosen exactly at R_{opt}^{LNA}=50Ω, since slight deviation of X_{opt}^{LNA} barely increases NF_{min}^{LNA}, so does R_{opt}^{LNA}. One can choose a smaller L_E like 50μm using correlation model for lower I_C.

$$X_{opt,Spice}^{LNA} = -\frac{\left(\frac{\omega_T}{\omega}\right)}{g_m}\frac{\frac{1}{\beta}\left(\frac{\omega_T}{\omega}\right)^2}{\left[1+\frac{1}{\beta}\left(\frac{\omega_T}{\omega}\right)^2\right]}, \tag{5.2}$$

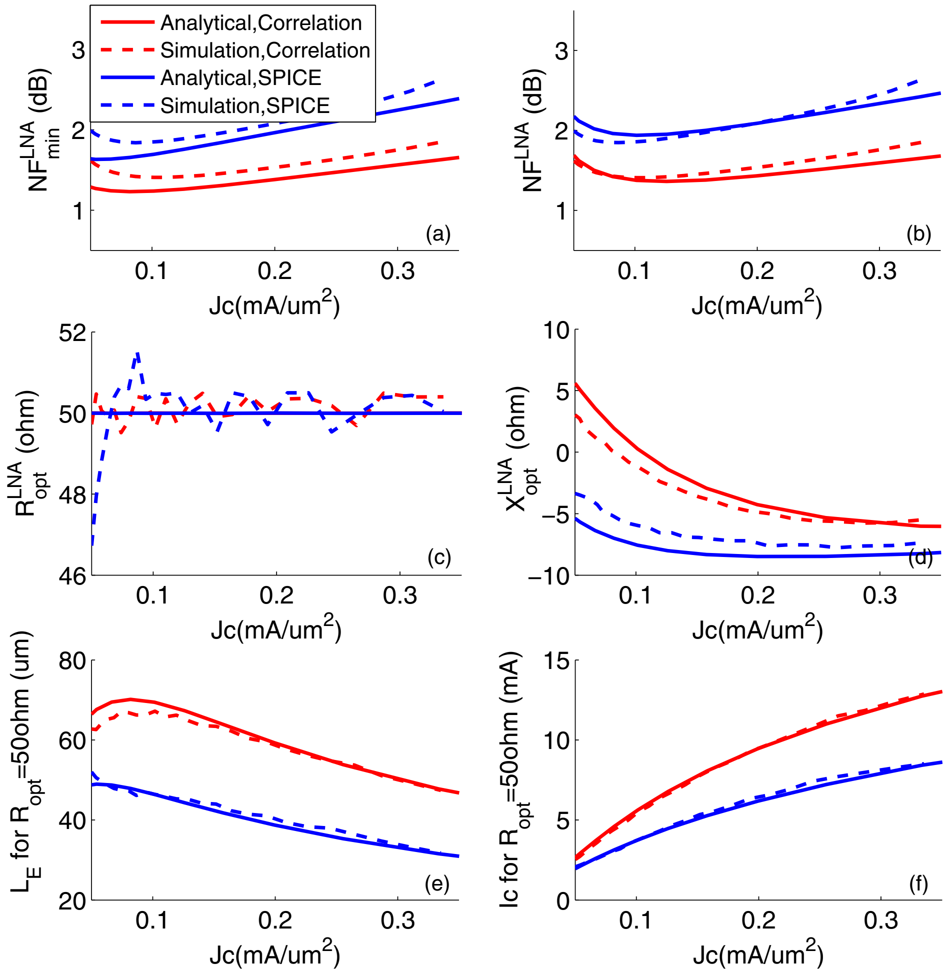

Figure 5.2: NF_{min}, NF, R_{opt}, X_{opt}, and corresponding L_E and I_C of LNAs using SPICE model and correlation model versus J_C at 5GHz.

$$X_{opt,cor}^{LNA} = -\frac{\left(\frac{\omega_T}{\omega}\right)}{g_m} \frac{\frac{1}{\beta}\left(\frac{\omega_T}{\omega}\right)^2 + (\omega_T\tau_n)^2 - (\omega_T\tau_n)}{\left[1 + \frac{1}{\beta}\left(\frac{\omega_T}{\omega}\right)^2 + (\omega_T\tau_n)^2 - 2(\omega_T\tau_n)\right]}. \tag{5.3}$$

Then we repeat LNA design at different J_C (V_{be}). Fig. 5.2 shows NF_{min}^{LNA}, NF^{LNA}, R_{opt}^{LNA}, and X_{opt}^{LNA}, and corresponding L_E and I_C with and without correlation versus J_C at 5GHz. The simulation data are generated using a cascode LNA [10][34]. The analytical curves agree well with simulation. In Fig. 5.2, X_{opt}^{LNA} with correlation is relatively closer to zero. X_{opt}^{LNA} without correlation is negative, i.e. (5.2), while X_{opt}^{LNA} with correlation is positive at small J_C, which agrees with analytical expressions, i.e. (5.3).

At every J_C bias, L_E is required to be rescaled. Although L_E could be chosen by optimizer in some simulator like Agilent ADS, it takes a plenty of time to generate one curve. By contrast, the L_E can be easily scaled for R_{opt}^{LNA}=50Ω in calculation. Thus, analytical approach improves the efficiency of LNA design.

Chapter 6

Technology Scaling

To investigate effect of technology scaling, we compare three lithography nodes $0.5\mu m$, $0.24\mu m$, and $0.13\mu m$. Parameters of the reference device are given in Table 6.1.

Table 6.1: Main Features of Three Technologies

Lithography Node (μm)	0.50	0.24	0.13
Peak f_T (GHz)	36	60	212
Peak f_{max} (GHz)	100	120	265
Working f (GHz)	6	10	35
Normalized r_b*L_E ($\Omega\mu m$)	412.9	341.4	210.8
Emitter area A_E (μm)	0.8×20×3	0.24×20×1	0.12×12×1

With increasing frequency, the contribution of $\frac{1}{\beta}$ in (4.2) and (4.3) is small [11]. (4.2) and (4.3) are simplified by neglecting contribution of $\frac{1}{\beta}$ except that in M:

$$R_{opt}^{Device} = r_b\sqrt{1 + \frac{2}{r_b g_m M}\left(\frac{\omega_T}{\omega}\right)^2}, \tag{6.1}$$

$$F_{min}^{Device} = 1 + r_b g_m M\left(\frac{\omega}{\omega_T}\right)^2\left[1 + \sqrt{1 + \frac{2}{r_b g_m M}\left(\frac{\omega_T}{\omega}\right)^2}\right], \tag{6.2}$$

where term $r_b g_m$ is independent of L_E for a given J_C, because $r_b \propto 1/L_E$ and $g_m \propto L_E$.

Fig. 6.1 shows f_T, NF_{min}^{Device}, and $r_b \times g_m$ versus J_C of three technologies. Because of different f_T, for a fair comparision, the J_C at which f_T=$f_{T,peak}/2$ in each technology is used. Since working frequency f is chosen as $f_{T,peak}/6$, ω_T/ω=3 in (6.1) and (6.2).

Fig. 6.2 shows NF_{min}^{Device} and $R_{opt}^{Device} \cdot L_E$ versus $r_b g_m$. The trends of NF_{min}^{Device} are consistent with $r_b g_m$: smaller $r_b g_m$ leads to smaller NF_{min}^{Device}. In (6.1), $R_{opt}^{Device} \cdot L_E$ is related with not only

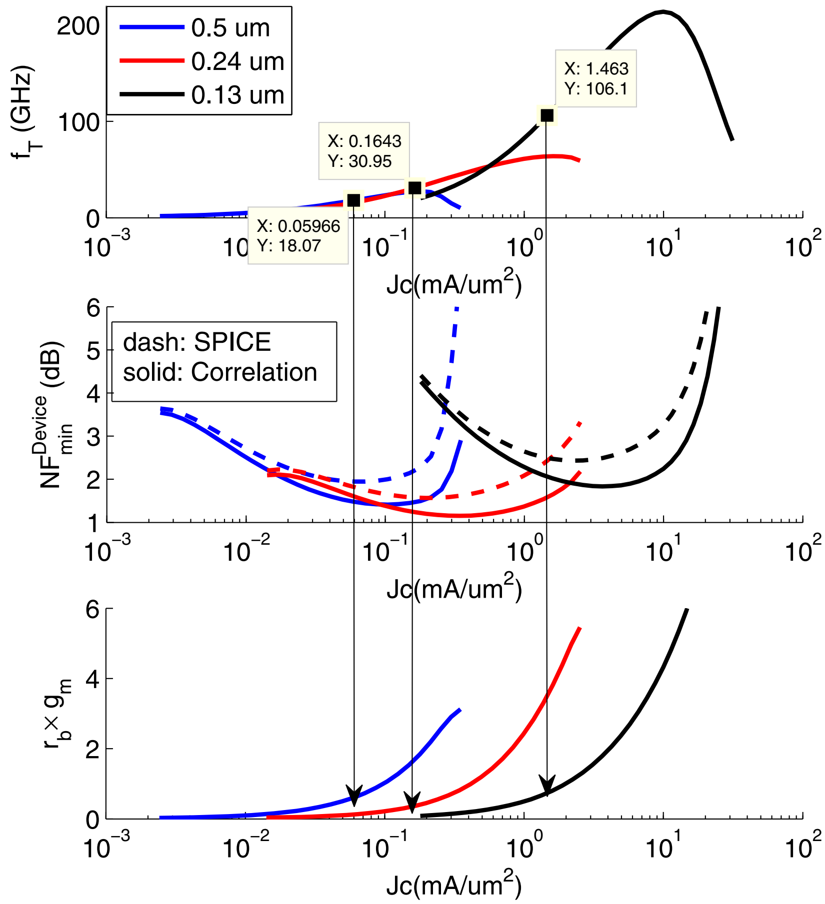

Figure 6.1: f_T, NF_{min}^{Device}, and $r_b \times g_m$ versus J_C of three technology devices.

$r_b g_m$, but also $r_b \cdot L_E$. The $0.13\mu m$ technology has much smaller $R_{opt}^{Device} \cdot L_E$ than the others, which will lead to smaller L_E in LNA design.

Fig. 6.3 shows L_E for noise matching and corresponding I_C and J_C versus lithography node in LNA design. Although J_C is highest at $0.13\mu m$ node, its smaller L_E requested for R_{opt}^{LNA}=50Ω and smaller W_E lead to less I_C since I_C=$L_E W_E J_C$. Despite the increasing J_C required to enable higher frequency design, the smaller L_E and W_E required for noise matching help keeping power consumption of LNA low.

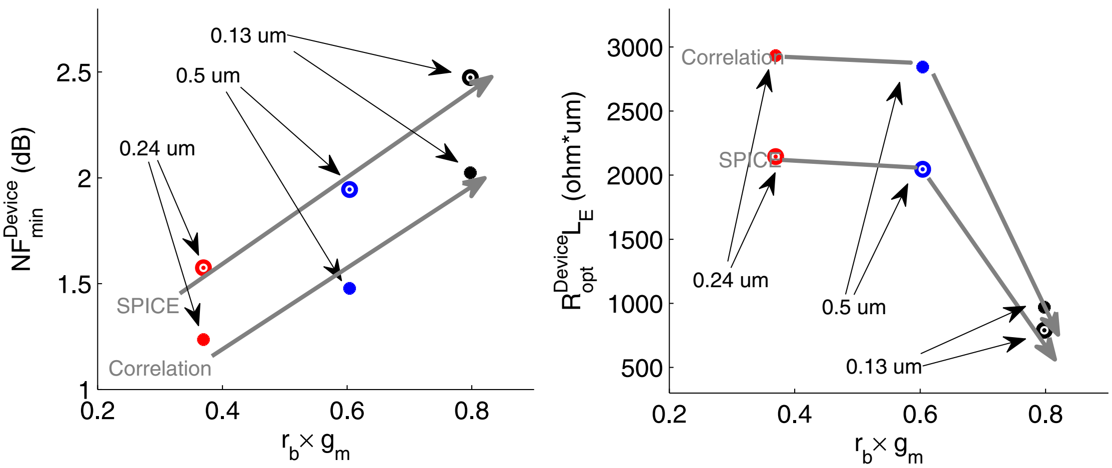

Figure 6.2: NF_{min}^{Device} and $R_{opt}^{Device} \cdot L_E$ versus $r_b \times g_m$ of three technology devices.

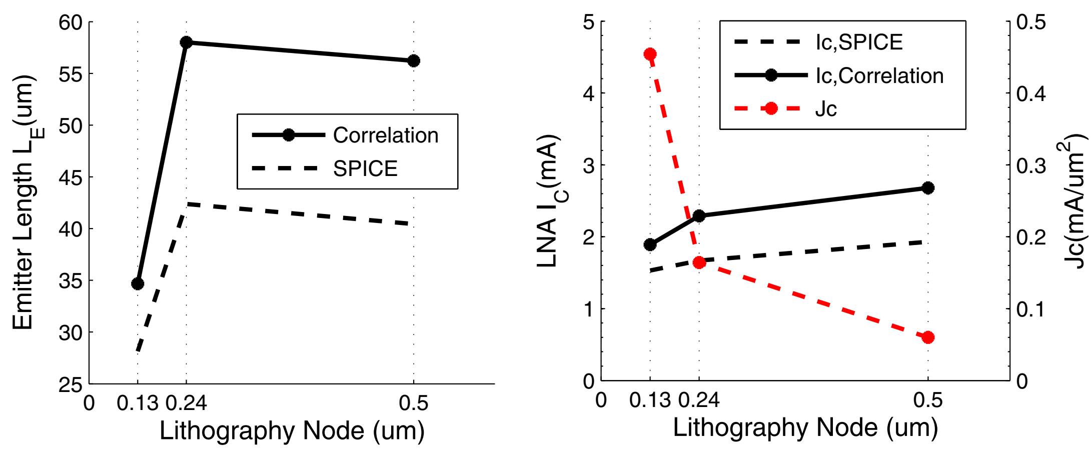

Figure 6.3: In LNA design, L_E, I_C, and J_C versus lithography node.

Chapter 7

Conclusion

The general analytical expressions of SiGe HBT and LNA noise parameters have been developed using small signal circuit analysis and verified by simulation and measurement data. The analytical expressions show that correlation leads to smaller NF_{min} and larger R_{opt} at a fixed emitter size. This impact depends on base resistance r_b, which plays more important role as an impedance than as a noise source for NF_{min}. Thus, r_b as impedance could not be neglected in analytical models. In LNA design, noise correlation leads to smaller NF_{min} and NF at a given bias, and better closeness of noise matching and impedance matching. Although a larger R_{opt} using correlation model leads to a larger L_E for LNA design, and a relatively higher I_C, L_E can be slightly adjusted for a good tradeoff that provides low power consumption, as well as low noise figure. Scaling of technology suggests that NF_{min} depends on $r_b g_m$ at the same f_T/f. Despite technology scaling required higher J_C for higher working frequency, shrunken W_E and L_E of transistor for noise matching keep I_C of LNA low.

Bibliography

[1] L. Escotte, J.-P. Roux, R. Plana, J. Graffeuil, and A. Gruhle, “Noise Modeling of Microwave Heteroiunction BiPolar Transistors,” *IEEE Transactions on Electron Devices*, vol. 42, pp. 883–889, May 1995.

[2] M. Rudolph, R. Doerner, L. Klapproth, and P. Heymann, “An HBT Noise Model Valid Up to Transit Frequency,” *IEEE Electron Device Letters*, vol. 20, pp. 24–26, Jan 1999.

[3] J. C. J. Paasschens, R. J. Havens, and L. F. Tiemeijer, “Modelling the Correlation in the High-Frequency Noise of (Hetero-junction) Bipolar Transistors using Charge-Partitioning,” *Proceedings of the Bipolar/BiCMOS Circuits and Technology Meeting*, pp. 221–224, Sept 2003.

[4] P. Sakalas, J. Herricht, A. Chakravorty, and M. Schroter, “Compact Modeling of High Frequency Correlated Noise in HBTs,” *Proceedings of the Bipolar/BiCMOS Circuits and Technology Meeting*, pp. 1–4, Oct 2006.

[5] A. van der Ziel, “Theory of Shot Noise in Junction Diodes and Junction Transistors,” *Proceedings of the IRE*, vol. 43, pp. 1639 – 1646, Nov 1955.

[6] K. Xia, G. Niu, D. Sheridan, and S. Sweeney, “Frequency and Bias-Dependent Modeling of Correlated Base and Collector Current RF Noise in SiGe HBTs Using Quasi-Static Equivalent Circuit,” *IEEE Transactions on Electron Devices*, vol. 53, pp. 515–522, March 2006.

[7] K. Yau and S. Voinigescu, “Modeling and Extraction of SiGe HBT Noise Parameters from Measured Y-Parameters and Accounting for Noise Correlation,” *Digest of IEEE Topical Meeting on Silicon Monolithic Integrated Circuits in RF Systems*, Jan 2006.

[8] Z. Xu, G. Niu, and R. M. Malladi, “Compact Modeling of Collector Base Junction Space Charge Region Transit Time Effect on Noise in SiGe HBTs,” *Digest of IEEE Topical Meeting on Silicon Monolithic Integrated Circuits in RF Systems*, pp. 180–183, Jan 2010.

[9] K. Yau, P. Chevalier, A. Chantre, and S. Voinigescu, “Characterization of the Noise Parameters of SiGe HBTs in the 70-170-GHz Range,” *IEEE Transactions on Microwave Theory and Techniques*, vol. 59, pp. 1983–2000, Aug 2011.

[10] P. Shen, G. Niu, Z. Xu, and W. Zhang, “Impact of High Frequency Correlated Noise on SiGe HBT Low Noise Amplifier Design,” *Digest of IEEE Topical Meeting on Silicon Monolithic Integrated Circuits in RF Systems*, pp. 125–128, Jan 2012.

[11] H. Fukui, “The Noise Performance of Microwave Transistors,” *IEEE Transactions on Electron Devices*, vol. 13, pp. 329–341, Mar 1966.

[12] S. P. Voinigescu, M. C. Maliepaard, J. L. Showell, G. E. Babcock, D. Marchesan, M. Schroter, P. Schvan, and D. L. Harame, “A Scalable High-frequency Noise Model for Bipolar Transistors with Application to Optimal Transistor Sizing for Low-noise Amplifier Design,” *IEEE Journal of Solid-State Circuits*, vol. 32, pp. 1430–1439, Sept 1997.

[13] J. D. Cressler and G. F. Niu, *Silicon-Germanium Heterojunction Bipolar Transistors*. Artech House, 2003.

[14] D. Greenberg, S. Sweeney, B. Jagannathan, G. Freeman, and D. Ahlgren, “Noise Performance Scaling in High-speed Silicon RF Technologies,” *Digest of IEEE Topical Meeting on Silicon Monolithic Integrated Circuits in RF Systems*, pp. 22–25, 2003.

[15] J.-S. Rieh, B. Jagannathan, D. Greenberg, M. Meghelli, A. Rylyakov, F. Guarin, Z. Yang, D. Ahlgren, G. Freeman, P. Cottrell, and D. Harame, “SiGe Heterojunction Bipolar Transistors and Circuits Toward Terahertz Communication Applications,” *IEEE Transactions on Microwave Theory and Techniques*, vol. 52, pp. 2390–2408, Oct. 2004.

[16] J. S. Rieh, D. Greenberg, A. Stricker, and G. Freeman, “Scaling of SiGe Heterojunction Bipolar Transistors,” *Proceedings of the IEEE*, vol. 93, pp. 1522–1538, Sept 2005.

[17] L. Larson, “Silicon Technology Tradeoffs for Radio-Frequency/Mixed-Signal "Systems-on-a-Chip",” *IEEE Transactions on Electron Devices*, vol. 50, pp. 683–699, March 2003.

[18] G. Niu, K. Xia, D. Sheridan, and D. L. Harame, “Experimental Extraction and Model Evaluation of Base and Collector Current RF Noise in SiGe HBTs,” *Digest of IEEE Radio Frequency Integrated Circuits Symposium*, pp. 615–618, 2004.

[19] Z. Xu and G. Niu, “Compact Modeling Based Extraction of RF Noise in SiGe HBT Terminal Currents,” *Digest of IEEE Topical Meeting on Silicon Monolithic Integrated Circuits in RF Systems*, pp. 137–140, Jan 2012.

[20] K. Xia and G. Niu, “Discussions and Extension of Van Vliet’s Noise Model for High Speed Bipolar Transistors,” *Solid-State Electronics*, vol. 53, pp. 349–354, March 2009.

[21] G. Niu, *Silicon Heterostructure Handbook*, ch. Microscopic Noise Simulation, pp. 459–474. Taylor and Francis, 2005.

[22] Y. Cui, G. Niu, and D. L. Harame, “An Examination of Bipolar Transistor Noise Modeling and Noise Physics Using Microscopic Noise Simulation,” *Proceedings of the Bipolar/BiCMOS Circuits and Technology Meeting*, pp. 225–228, Sept 2003.

[23] K. Xia, G. Niu, and Z. Xu, “A New Approach to Implementing High-Frequency Correlated Noise for Bipolar Transistor Compact Modeling,” *IEEE Transactions on Electron Devices*, vol. 59, pp. 302–308, Feb 2012.

[24] O. Shana'A, I. Linscott, and L. Tyler, "Frequency-scalable SiGe Bipolar RFIC Front-end Design," *Proceedings of the IEEE*, pp. 183–186, May 2000.

[25] J. Cressler, "SiGe HBT Technology: A New Contender for Si-based RF and Microwave Circuit Applications," *IEEE Transactions on Microwave Theory and Techniques*, vol. 46, pp. 572–589, May 1998.

[26] Z. Xu, *Physics, Modeling and Design Implications of RF Correlated Noise in SiGe HBTs*. Auburn University, 2013.

[27] L. Luo, *Physics, Compact Modeling and TCAD of SiGe HBT for Wide Temperature Range Operation*. Auburn University, 2011.

[28] G. Niu, J. Cressler, S. Zhang, W. Ansley, C. Webster, and D. Harame, "A Unified Approach to RF and Microwave Noise Parameter Modeling in Bipolar Transistors," *IEEE Transactions on Electron Devices*, vol. 48, pp. 2568–2574, Nov 2001.

[29] F. Bonani and G. Ghione, *Noise in Semiconductor Devices: Modeling and Simulation*. Springer, 2001.

[30] M. Reisch, *High-Frequency Bipolar Transistors*. Springer, 2003.

[31] H. Haus, W. Atkinson, G. Branch, W. Davenport, W. Fonger, W. Harris, S. Harrison, W. McLeod, E. Stodola, and T. Talpey, "Representation of Noise in Linear Twoports," *Proceedings of the IRE*, vol. 48, pp. 60–74, Jan 1960.

[32] Y. Chen, X. Yuan, D. Scagnelli, J. Mecke, J. Gross, and D. Harame, "Demonstration of a SiGe RF LNA Design Using IBM Design Kits in 0.18 μm SiGe BiCMOS Technology," *Proceedings of Design, Automation and Test in Europe Conference and Exhibition*, vol. 3, pp. 22–27, Feb 2004.

[33] M. Schröter and D. J. Walkey, "Physical Modeling of Lateral Scaling in Bipolar Transistors," *IEEE Journal of Solid-State Circuits*, vol. 31, pp. 1484–1492, Oct 1996.

[34] Q. Liang, G. Niu, J. D. Cressler, S. Tayler, and D. L. Harame, "Geometry and Bias Current Optimization for SiGe HBT Cascode Low-Noise Amplifiers," *IEEE MTT-S International Microwave Symposium Digest*, vol. 1, pp. 517–520, Jun 2002.

Appendices

Appendix A

Derivation of Intrinsic Noise Sources' Contributions to i_{out}:

i^c_{out}, i^b_{out}, i^{rb}_{out}, and i^{Rs}_{out}

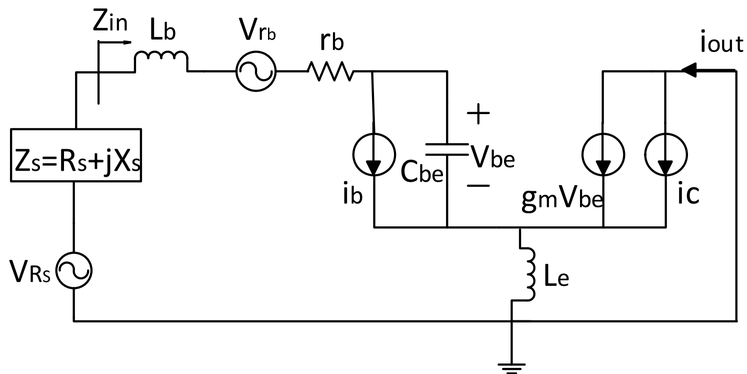

Figure A.1: Simplified small signal equivalent circuit of LNA

Fig. A.1 is small signal equivalent circuit of LNA with all noise sources. The transistor noise sources include the terminal current noises i_c and i_b, and the thermal noises v_b of r_b. Power source has a noise source v_s of Z_s. i^c_{out}, i^b_{out}, i^{rb}_{out}, and i^{Rs}_{out} are denoted as contributions of i_c, i_b, v_b, and v_s to total output noise current i_{out}, respectively. Each could be calculated using circuit analysis by removing the other noise sources in Fig. A.1.

A.0.1 i^c_{out}:

i^c_{out} could be calculated by circuit analysis using Fig. A.2, which includes only one noise source, i.e. i_c.

$$V^c_{be} \cdot j\omega C_{be} \left[Z_s + r_b + j\omega(L_b + L_e) \right] + V^c_{be} + j\omega(i_c + g_m V^c_{be}) L_e = 0. \tag{A.1}$$

Then,

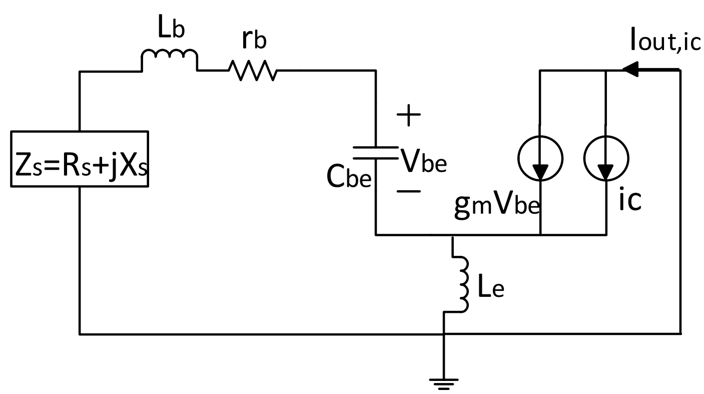

Figure A.2: Simplified small signal equivalent circuit of LNA with intrinsic current noise source i_c.

$$V_{be}^{c} = -j\omega i_c L_e \cdot \frac{1}{\alpha}, \tag{A.2}$$

where

$$\alpha = 1 - \omega^2 C_{be}(L_b + L_e) + j\omega C_{be}(Z_s + r_b) + j\omega g_m L_e. \tag{A.3}$$

Therefore,

$$i_{out}^{c} = V_{be}^{c} \cdot g_m + i_c = -j\omega g_m i_c L_e \cdot \frac{1}{\alpha} + i_c, \tag{A.4}$$

A.0.2 i_{out}^{b}:

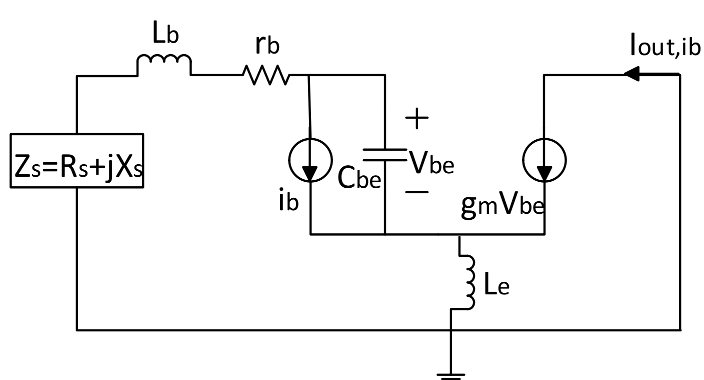

Figure A.3: Simplified small signal equivalent circuit of LNA with intrinsic current noise source i_b.

i_{out}^{b} could be calculated by circuit analysis using Fig. A.3, which includes only one noise source, i.e. i_b:

$$V_{be}^{b} = -i_b\left[(Z_s + r_b) + j\omega(L_b + L_e)\right] \cdot \frac{1}{\alpha}, \tag{A.5}$$

$$i_{out}^{b} = V_{be}^{b} \cdot g_m = -g_m i_b\left[(Z_s + r_b) + j\omega(L_b + L_e)\right] \cdot \frac{1}{\alpha}. \tag{A.6}$$

A.0.3 i_{out}^{rb}:

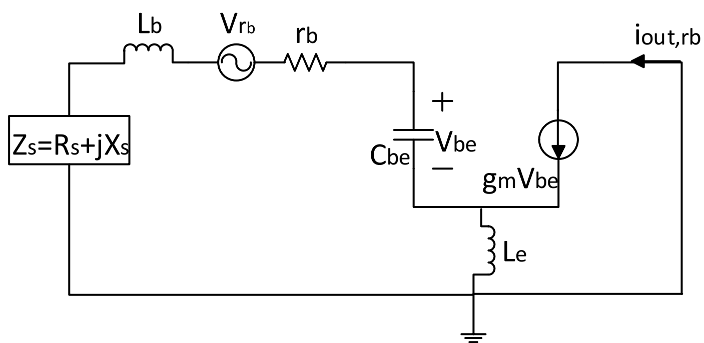

Figure A.4: Simplified small signal equivalent circuit of LNA with thermal noise source v_{rb}.

i_{out}^{rb} could be calculated by circuit analysis using Fig. A.4, which includes only one noise source, i.e. v_{rb}:

$$V_{be}^{rb} = -v_{rb} \cdot \frac{1}{\alpha}, \tag{A.7}$$

$$i_{out}^{rb} = V_{be}^{rb} \cdot g_m = -g_m v_{rb} \cdot \frac{1}{\alpha}. \tag{A.8}$$

A.0.4 i_{out}^{Rs}:

i_{out}^{Rs} could be calculated by circuit analysis using Fig. A.2, which includes only one noise source, i.e. v_{Rs}:

$$V_{be}^{Rs} = v_{Rs} \cdot \frac{1}{\alpha}, \tag{A.9}$$

$$i_{out}^{Rs} = V_{be}^{Rs} \cdot g_m = g_m v_{Rs} \cdot \frac{1}{\alpha}. \tag{A.10}$$

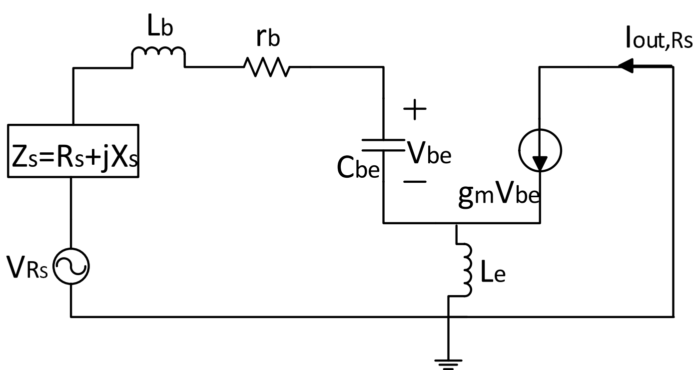

Figure A.5: Simplified small signal equivalent circuit of LNA with thermal noise source v_{Rs}.

Appendix B

Matlab Code for Noise Parameters of Device Calculation

```
close all;
clear all;

format long;
datapath =
'C:\Users\Xiaojia\Documents\Iccap\Noise\Noise5PAE_Hicum\7WLNoise_wrk\export_d
ata\';

OPinfo = sprintf('%s7WL_p24_OPinfo.csv',datapath);
OPinfo_wt = sprintf('%s7WL_p24_OPinfo_wt.csv',datapath);

[OP] = textread(OPinfo,'','delimiter',',','headerlines',46);
%'Vbe','0Hz','1','OP_betadc','OP_ib','OP_ic','OP_rb','OP_Cbe','OP_taun'
[OP_wt] = textread(OPinfo_wt,'','delimiter',',','headerlines',36);
%'','','','wt_gm','','','wt_fT'

[Ic] = OP(:,6)';
[rb] = OP(:,7)';
[Cbe] = OP(:,8)';
[beta] = OP(:,4)';
[taun] = OP(:,9)';
[wt] = OP_wt(:,7)';

freq = 10e9;

Length_e0 = 1 * 20;
Width_e = 0.24;
Ae = Width_e * Length_e0;

q = 1.602189e-19;
twoq = 2 * q;
w = 2 * pi * freq;
Temp = 290;
```

```
k = 1.380662e-23;
kt = k * Temp;

m = size(Ic,2);
for n = 1:m
    Cbe_bc(n) = Cbe(n);
    Ib(n) = Ic(n)/beta(n);
    gm(n) = wt(n)*Cbe_bc(n);
    wCbe_inv(n) = 1/(w * Cbe_bc(n));
    wt_w(n) = wt(n)/w;
    Jc(n) = Ic(n)/Ae;

    fg1 = 0.757;
    T(n) = taun(n)*fg1;

    %%-----------------------------correlation----------------------------
    Sib(n) = twoq * Ib(n) + twoq * Ic(n) * (w * T(n)).^2;
    Sic(n) = twoq * Ic(n);
    Bu(n) = -twoq * Ic(n) * w * T(n);

    AA(n) = Sic(n) + Sib(n) * wt_w(n).^2 + 2 * Bu(n) * wt_w(n);

    Xopt(n) = wCbe_inv(n) * (Sic(n) + Bu(n) * wt_w(n))/AA(n);% - wCbe_inv(n);
% "- wCbe_inv(n)" for LNA
    Ropt2(n) = 4*kt * rb(n) * wt_w(n).^2/AA(n) + rb(n).^2 + wCbe_inv(n).^2 *
Sic(n)/AA(n) - wCbe_inv(n).^2 * (Sic(n) + Bu(n) * wt_w(n)).^2/(AA(n).^2);
    Ropt(n) = sqrt(Ropt2(n));
    Fmin(n) = 1 + rb(n)/Ropt(n) + 1/(4 * kt * Ropt(n)) * (1/wt_w(n)).^2 *
(Ropt(n) + rb(n)).^2 * AA(n) + 1/(4 * kt * Ropt(n)) * wCbe_inv(n).^2 *
(Sic(n) * Sib(n) - Bu(n).^2) / AA(n) ;
    NFmin(n) = 10*log10(Fmin(n));

    R(n) = (50+rb(n)).^2+0.^2;
    F(n) = 1+rb(n)/50+Sic(n)*(1+(w*Cbe_bc(n)).^2*R(n)-
2*w*Cbe_bc(n)*0)/(gm(n).^2*4*kt*50)+Sib(n)*R(n)/(4*kt*50)-
2*Bu(n)*0/(gm(n)*4*kt*50)+2*Bu(n)*w*Cbe_bc(n)*R(n)/(gm(n)*4*kt*50);
```

```
    NF(n) = 10*log10(F(n));

    C(n) = 1 + (w * Cbe_bc(n) * rb(n)).^2;

    Iout_icib(n) = twoq * Ic(n) + (twoq * Ib(n) + twoq * Ic(n) * (w *
T(n)).^2) * gm(n).^2 * rb(n).^2/C(n) + 2 * Bu(n) * gm(n) * w * Cbe_bc(n) *
rb(n).^2/C(n);

    Iout_rb(n) = 4*kt * rb(n) *gm(n).^2/C(n);
    Iout(n) = Iout_icib(n) + Iout_rb(n);
    Y21_inv(n) = (1 + j * w * Cbe_bc(n) * rb(n))/gm(n);
    Sva(n) = Iout(n)*(abs(Y21_inv(n))).^2;
    Rn(n) = Sva(n)/(4*kt);

    %%-----------------------------spice----------------------
    Sib_spice(n) = twoq * Ib(n);
    Sic_spice(n) = twoq * Ic(n);
    Bu_spice(n) = 0;

    AA_spice(n) = Sic_spice(n) + Sib_spice(n) * wt_w(n).^2 + 2 * Bu_spice(n)
* wt_w(n);

    Xopt_spice(n) = wCbe_inv(n) * (Sic_spice(n) + Bu_spice(n) *
wt_w(n))/AA_spice(n);% - wCbe_inv(n);        % "- wCbe_inv(n)" for LNA
    Ropt2_spice(n) = 4*kt * rb(n) * wt_w(n).^2/AA_spice(n) + rb(n).^2 +
wCbe_inv(n).^2 * Sic_spice(n)/AA_spice(n) - wCbe_inv(n).^2 * (Sic_spice(n) +
Bu_spice(n) * wt_w(n)).^2/(AA_spice(n).^2);
    Ropt_spice(n) = sqrt(Ropt2_spice(n));
    Fmin_spice(n) = 1 + rb(n)/Ropt_spice(n) + 1/(4 * kt * Ropt_spice(n)) *
(1/wt_w(n)).^2 * (Ropt_spice(n) + rb(n)).^2 * AA_spice(n) + 1/(4 * kt *
Ropt_spice(n)) * wCbe_inv(n).^2 * (Sic_spice(n) * Sib_spice(n) -
Bu_spice(n).^2) / AA_spice(n) ;
    NFmin_spice(n) = 10*log10(Fmin_spice(n));

    R_spice(n) = (50+rb(n)).^2+0.^2;
```

```
    F_spice(n) = 1+rb(n)/50+Sic_spice(n)*(1+(w*Cbe_bc(n)).^2*R_spice(n)-
2*w*Cbe_bc(n)*0)/(gm(n).^2*4*kt*50)+Sib_spice(n)*R_spice(n)/(4*kt*50)-
2*Bu_spice(n)*0/(gm(n)*4*kt*50)+2*Bu_spice(n)*w*Cbe_bc(n)*R_spice(n)/(gm(n)*4
*kt*50);
    NF_spice(n) = 10*log10(F_spice(n));

    C(n) = 1 + (w * Cbe_bc(n) * rb(n)).^2;

    Iout_icib_spice(n) = twoq * Ic(n) + (twoq * Ib(n)) * gm(n).^2 *
rb(n).^2/C(n) + 2 * Bu_spice(n) * gm(n) * w * Cbe_bc(n) * rb(n).^2/C(n);

    Iout_rb(n) = 4*kt * rb(n) *gm(n).^2/C(n);
    Iout_spice(n) = Iout_icib_spice(n) + Iout_rb(n);
    Y21_inv(n) = (1 + j * w * Cbe_bc(n) * rb(n))/gm(n);
    Sva_spice(n) = Iout_spice(n)*(abs(Y21_inv(n))).^2;
    Rn_spice(n) = Sva_spice(n)/(4*kt);
end

 figure(1);

 subplot(4,1,1); hold on;
 plot(Jc*1e3,NFmin,'r-','LineWidth',2);
 plot(Jc*1e3,NFmin_spice,'r--','LineWidth',2);
 xlabel('Jc(mA/um^2)');ylabel('NF^{Device}_{min} (dB)');

 subplot(4,1,2); hold on;
 plot(Jc*1e3,Ropt,'r-','LineWidth',2);
 plot(Jc*1e3,Ropt_spice,'r--','LineWidth',2);
 xlabel('Jc(mA/um^2)');ylabel('R^{Device}_{opt} (ohm)');

 subplot(4,1,3); hold on;
 plot(Jc*1e3,Xopt,'r-','LineWidth',2);
 plot(Jc*1e3,Xopt_spice,'r--','LineWidth',2);
 xlabel('Jc(mA/um^2)');ylabel('X^{Device}_{opt} (ohm)');

 subplot(4,1,4); hold on;
```

```
plot(Jc*1e3,Rn./50,'r-','LineWidth',2);
plot(Jc*1e3,Rn_spice./50,'r--','LineWidth',2);
xlabel('Jc(mA/um^2)');ylabel('R^{Device}_{n}/50');
```

Appendix B

Matlab Code for Noise Parameters of Matched LNA

```
close all;
clear all;

format long;
datapath =
'C:\Users\Xiaojia\Documents\Iccap\Noise\Noise5PAE_Hicum\7WLNoise_wrk\export_d
ata\';

OPinfo = sprintf('%s7WL_p24_OPinfo.csv',datapath);
OPinfo_wt = sprintf('%s7WL_p24_OPinfo_wt.csv',datapath);

[OP] = textread(OPinfo,'','delimiter',',','headerlines',46);
%'Vbe','0Hz','1','OP_betadc','OP_ib','OP_ic','OP_rb','OP_Cbe','OP_taun'
[OP_wt] = textread(OPinfo_wt,'','delimiter',',','headerlines',36);
%'','','','wt_gm','','','wt_fT'

[Ic] = OP(:,6)';
[rb] = OP(:,7)';
[Cbe] = OP(:,8)';
[beta] = OP(:,4)';
[taun] = OP(:,9)';
[wt] = OP_wt(:,7)';
freq = 10e9;

Length_e0 = 1 * 20;
Width_e = 0.24;
Ae = Width_e * Length_e0;

q = 1.602189e-19;
twoq = 2 * q;
w = 2 * pi * freq;
T = 290;
k = 1.380662e-23;
```

```
kt = k * T;

rb_per_um = rb * Length_e0;
Ic_per_um = Ic/Length_e0;
Cbe_per_um = Cbe/Length_e0;

m = size(Ic,2);
for n = 1:m

    Jc(n) = Ic(n)/Ae;
    Ropt(n) = 100;
    Length_e(n) = 1;

    while (Ropt(n) >= 50)

        Length_e(n) = Length_e(n) + 0.01;

        rb_2(n) = rb_per_um(n) / Length_e(n);
        Ic_2(n) = Ic_per_um(n) * Length_e(n);
        Cbe_2(n) = Cbe_per_um(n) * Length_e(n);

        Ae_2(n) = Length_e(n) * Width_e;
        Ib(n) = Ic_2(n)/beta(n);
        gm(n) = wt(n)*Cbe_2(n);

        wCbe_inv(n) = 1/(w * Cbe_2(n));
        wt_w(n) = wt(n)/w;

        fg1 = 0.757;
        T(n) = taun(n)*fg1;

        Sib(n) = twoq * Ib(n) + twoq * Ic_2(n) * (w * T(n)).^2;
        Sic(n) = twoq * Ic_2(n);
        Sicib(n) = -j * twoq * Ic_2(n) * w * T(n);
        Bu(n) = -twoq * Ic_2(n) * w * T(n);
```

```
        AA(n) = Sic(n) + Sib(n) * wt_w(n).^2 + 2 * Bu(n) * wt_w(n);

        Ropt2(n) = 4*kt * rb_2(n) * wt_w(n).^2/AA(n) + rb_2(n).^2 +
wCbe_inv(n).^2 * Sic(n)/AA(n) - wCbe_inv(n).^2 * (Sic(n) + Bu(n) *
wt_w(n)).^2/(AA(n).^2);
        Ropt(n) = sqrt(Ropt2(n));

    end

    Xopt(n) = wCbe_inv(n) * (Sic(n) + Bu(n) * wt_w(n))/AA(n) - wCbe_inv(n);

    Fmin(n) = 1 + rb_2(n)/Ropt(n) + 1/(4 * kt * Ropt(n)) * (1/wt_w(n)).^2 *
(Ropt(n) + rb_2(n)).^2 * AA(n) + 1/(4 * kt * Ropt(n)) * wCbe_inv(n).^2 *
(Sic(n) * Sib(n) - Bu(n).^2) / AA(n) ;
    NFmin(n) = 10*log10(Fmin(n));

    R(n) = (50+rb_2(n)).^2+0.^2;
    F(n) = 1+rb_2(n)/50+Sic(n)*(1+(w*Cbe_2(n)).^2*R(n)-
2*w*Cbe_2(n)*0)/(gm(n).^2*4*kt*50)+Sib(n)*R(n)/(4*kt*50)-
2*Bu(n)*0/(gm(n)*4*kt*50)+2*Bu(n)*w*Cbe_2(n)*R(n)/(gm(n)*4*kt*50);
    NF(n) = 10*log10(F(n));

    C(n) = 1 + (w * Cbe_2(n) * rb_2(n)).^2;

    Iout_icib(n) = twoq * Ic_2(n) + (twoq * Ib(n) + twoq * Ic(n) * (w *
T(n)).^2) * gm(n).^2 * rb_2(n).^2/C(n) + 2 * Bu(n) * gm(n) * w * Cbe_2(n) *
rb_2(n).^2/C(n);

    Iout_rb(n) = 4*kt * rb_2(n) *gm(n).^2/C(n);
    Iout(n) = Iout_icib(n) + Iout_rb(n);
    Y21_inv(n) = (1 + j * w * Cbe_2(n) * rb_2(n))/gm(n);
    Sva(n) = Iout(n)*(abs(Y21_inv(n))).^2;
    Rn(n) = Sva(n)/(4*kt);

end
```

```
figure(1);

 subplot(2,2,1); hold on;
 plot(Jc*1e3,NFmin,'r-','LineWidth',2);
 xlabel('Jc(mA/um^2)');ylabel('NFmin(dB)');

 subplot(2,2,2); hold on;
 plot(Jc*1e3,NF,'r-','LineWidth',2);
 xlabel('Jc(mA/um^2)');ylabel('NF(dB)');

 subplot(2,2,3); hold on;
 plot(Jc*1e3,Ropt,'r-','LineWidth',2);
 xlabel('Jc(mA/um^2)');ylabel('Ropt(ohm)');

 subplot(2,2,4); hold on;
 plot(Jc*1e3,Xopt,'r-','LineWidth',2);
 xlabel('Jc(mA/um^2)');ylabel('Xopt(ohm)');
```